The Dissertation Committee for Minxi Jiang
certifies that this is the approved version of the following dissertation:

Adiabatic Dynamics of Low-Lying Collective Modes in the BEC-BCS Crossover

Committee:

Qian Niu, Supervisor

Harry Swinney

Roger Bengtson

Gennady Shvets

Lorenzo A. Sadun

Adiabatic Dynamics of Low-Lying Collective Modes in the BEC-BCS Crossover

by

Minxi Jiang, B.S.

DISSERTATION

Presented to the Faculty of the Graduate School of

The University of Texas at Austin

in Partial Fulfillment

of the Requirements

for the Degree of

DOCTOR OF PHILOSOPHY

THE UNIVERSITY OF TEXAS AT AUSTIN

August 2011

To my parents,

and my husband,

for their unconditional love.

Acknowledgments

I would like to express my sincere gratitude toward my Ph. D. advisor Dr. Qian Niu, for his clear guidance and long-term support of my graduate research over these years. His deep insight and far-reaching vision in physics have inspired me again and again when I was stuck with difficulties and confusions.

It is my great pleasure to thank Dr. Roger Bengtson, whom I have been working with as a teaching assistant for four years. I thank him for his endless supports and wise advises as a great friend.

I would like to extend my appreciation to all the other members on my graduate committee, Dr. Harry Swinney, Dr. Ken Shih, Dr. Gennady Shvets and Dr. Lorenzo A. Sadun, for providing critical suggestions in writing this dissertation.

My thanks also go to Dr. Takeshi Udagawa and Dr. John Keto, the two successive graduate advisers, for all the invaluable advices they gave me and for being patient and friendly when I kept on bothering them with many tedious matters.

Finally, I would like to thank my parents and my husband with all my heart. They love me for who I am. Their love accompanied me through the valleys and hills in my life.

Adiabatic Dynamics of Low-Lying Collective Modes in the BEC-BCS Crossover

Publication No. _____

Minxi Jiang, Ph.D.
The University of Texas at Austin, 2011

Supervisor: Qian Niu

As the hydrodynamic theory breaks down with the local density approximation in the fermionic superfluid with spin-polarization, we develop a general formalism of the adiabatic dynamics for the low-lying collective modes in the BEC-BCS crossover, which is exact in the adiabatic limit. This adiabatic dynamic theory is based on a static density functional theory of the spin-polarized superfluid system, which we derive as a generalization of the conventional density functional theory of superfluid for current experimental interests. A special case where the system is uniform and analytically solvable is studied in detail. We show that our adiabatic equations of motion are reduced to the hydrodynamic equations of motion within local density approximation, which provides a solid microscopic foundation for the well-publicized phenomenological hydrodynamic theory.

Table of Contents

List of Figures

Chapter 1

Introduction to BEC-BCS Crossover

It is well known that all elementary particles can be divided into two basic categories depending on their spins, bosons and fermions. The bosons are particles with integer spins. They obey the Bose-Einstein statistics, which means that an unlimited number of bosons may simultaneously share a single quantum state. Therefore, when the temperature is cooled close to absolute zero, a finite fraction of bosons would stay in the same lowest quantum state. This new state of matter is called Bose-Einstein Condensation (BEC).

BEC owes its name to the prediction of physicists Bose and Einstein [1, 2] in 1925. The well-publicized experimental realization of BEC in 1995 [3, 4, 5] (seventy years after its theoretical predication) has fundamental significance in modern physics. The velocity-distribution of the trapped atoms are shown in Figure 1.1, which is one of the most well-known images of BEC. The number of atoms sharing the same velocity is indicated by the false color in the image, varying from the fewest (red) to the most (white). A sharp peak appears when the system is cooled below a critical temperature, confirming the formation of BEC for the first time.

In contrast to the condensation of bosons, it is much more difficult to

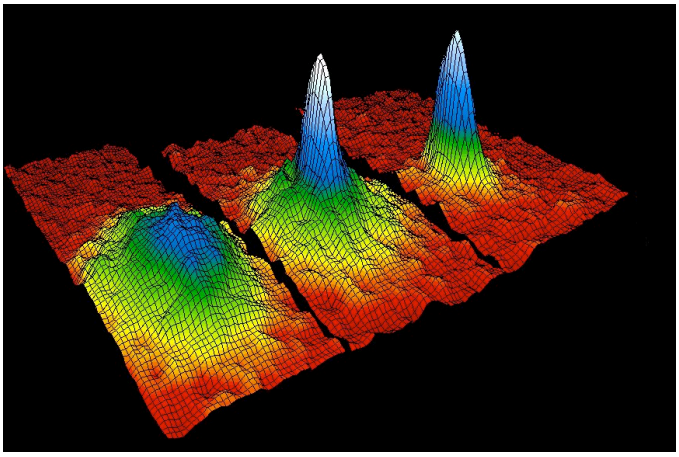

Figure 1.1: Velocity-distribution of a dilute rubidium gas, as an ambiguous proof of the discovery of BEC, with the system just above the critical temperature (left); just below the critical temperature (middle); after further cooling (right). Images courtesy of Mike Matthews, JILA research team.

generate a fermionic condensate, because the Pauli exclusion principle would prevent the fermions to occupy the same quantum state simultaneously. However, there are two

However, there are two seemingly very different mechanisms by which a condensate phase may be formed out of fermionic particles. The first one is a direct generalization of the condensation of bosons. If the fermions in the system could be paired up and strongly bound together in a way that the pair size is much smaller than the average interparticle spacing, it is good enough to ignore the underlying fermionic statistic and regard the fermion pair as a boson. Then, the composite boson should be condensed in the same way as the normal bosons. The second way to condense the fermions is based

on the well-known BCS theory of superconductivity [6]. Fermions can pair up as Cooper pairs [7] in the presence of a weak attractive interaction. The condensation of these Cooper pairs occurs simultaneously with the formation process. The Cooper pairs are huge whose size is typically orders of magnitude larger (100 times in conditional superconductors) than the average spacing between fermions. They cannot be thought of as separate bosons since there can be other fermions in between the two fermions of a Cooper pair. In recent experiments [8, 9, 10, 11, 12, 13, 14] it was found that the fermionic condensate can be achieved not only in the cases mentioned above, but along a whole crossover between BEC and BCS as the two limits (Figure 1.2). This whole range which smoothly connect the two regimes of BEC of bound molecules and BCS of Cooper pairs is called BEC-BCS crossover [15].

A crucial tool to achieve the BEC-BCS crossover is the Feshbach resonance [17, 18, 19], which permits one to change the two-body interaction between fermions simply by tuning an external magnetic field B. At low enough temperatures, the interaction between two fermions can be described by a single parameter, the s-wave scattering length a. Through Feshbach resonance, the value and even the sign of a can be adjust continuously along the crossover from the BEC limit (where a is small and positive), through the unitary limit (where a is order of magnitudes larger than the interparticle distance), to the BCS limit (where a is small and negative). The relation between a and B is given by

$$a \propto -\frac{1}{B - B_0} \tag{1.1}$$

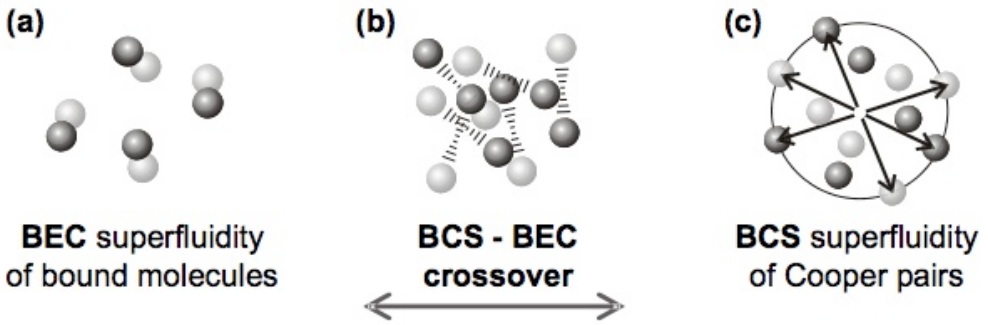

Figure 1.2: Pairing mechanisms of fermions: (a) The BEC side, the fermions form bound molecules whose sizes are smaller than the typical interparticle spacings, (c) The BCS side, Cooper pairs are formed on the fermi surface with the pair sizes much larger than the typical interparticle spacings, (b) The crossover in between, the paired up fermions can be regarded as generalized Cooper pairs whose sizes are in the same order of interparticle spacings. This figure is a reproduction of Fig. 5 given in [16].

with B_0 the critical magnetic field where the Feshbach resonance takes place. The whole region of BEC-BCS crossover has two sides and three limits which are widely mentioned in the literature. On the one side where $a > 0$, the fermions prefer to form bound molecules which undergo BEC to superfluidity at low temperature. This side of the resonance is called "BEC-side". On the other side of the resonance where $a < 0$, fermions tend to form loosely bound Cooper pairs which simultaneously condense and form a superfluid. This side is called "BCS-side". The three limits are the BEC limit, the BCS limit, and the unitary limit, which are corresponding to the scattering length $a \to 0^+$, $a \to 0^-$ and $a \to \infty$, respectively.

The BEC-BCS crossover arouses considerable interests in the physics

community. A comparative study of fermi and bose condensation enables one to investigate the role of quantum statistics at low temperature in a more comprehensive way. BEC-BCS crossover also serves as the first highly controllable testbed for theories of strongly correlated many-body system. Also, the superfluidity at the strong-interacting unitary limit is associated with a new form of superfluidity that may provide insights into high-temperature superconductivity [20, 21] (in the sense that $T_c/T_F \approx 0.2$). Moreover, with the study of BEC-BCS crossover, one can learn about the strongly interacting fermi gas, which maybe a probe to explore the physics of the high density nuclear matter found in the center of neutron star [22].

In the next chapter, I will review the dynamical behavior of BEC-BCS crossover from both an experimental and a theoretical point of view.

Chapter 2

Dynamics of the Ultra-Cold Fermi Gas

In this chapter, we will briefly review the dynamics of ultra-cold fermi atoms in the BEC-BCS crossover from both an experimental and a theoretical point of view. We will mainly focus on the low-lying collective modes. Many relevant experiments have been conducted to investigate the dynamical properties [23, 24, 25, 26, 27]. On the theoretical side, a major achievement is the phenomenological hydrodynamic theory [26, 28], which has proven capable to describe most of the relevant experimentally measured quantities with high accuracy. Yet a solid microscopic foundation for the hydrodynamic theory is missing, which is a major motivation we hope to systematically develop a dynamical theory for the BEC-BCS crossover in the microscopic framework.

2.1 Experimental measurements

The time-dependent behaviors of fermi condensates are important sources of information about the physical nature of the condensate. In this section, we summarize experiments of the dynamical behaviors in the BEC-BCS crossover region: anisotropic expansion and low-lying collective modes.

2.1.1 Anisotropic expansion

Most of our knowledge about the properties of fermi condensates comes from the density distribution images recorded from the absorption imaging technique [29]. The absorption images are often taken after some free expansion of the cloud from the confining trap, since the density of the initial trapped cloud is so high that the absorption is strongly saturated. It is essential to study the dynamics of fermi condensate which allows us to recover the information of the original atomic cloud from the density distribution after some free expansion. As in figure 1.1, the velocity distribution of the fermi condensate is extracted from the spatial distribution of the atoms recorded in the absorption image after a certain time of free-expansion (1/20 second). Besides, the free expansion is significant by itself since it reveals information about the interactions between fermions.

Figure 2.1 shows images of the anisotropic expansion of the degenerate gas over a time period of 2.0 ms. The ultra-cold fermi cloud is initially trapped by an anisotropic potential with stronger confinement in the radial direction, therefore the shape of the fermionic condensate is cigar-like. After a sudden release of the confining trap, the condensate begins to expand. One can see that the condensate expands faster in the radial direction, and it is converted into a disk-like shape after 2.0 ms. This anisotropic expansion of fermi condensate differs dramatically from the isotropic expansion of the non-interacting thermal cloud. Due to the isotropy of the velocity (momentum) distribution, the asymptoticly expanding shape of a thermal cloud will be isotropic, and the

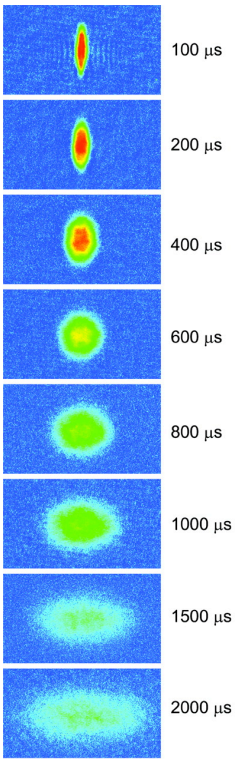

Figure 2.1: Snapshots of the free expansion of ^{6}Li fermionic condensate, taken at different times after released from the confining trap. The shape of the originally cigar-like fermion condensate eventually becomes disk-like after the anisotropic expansion. This figure is a reproduction of Figure 1 in [23].

final aspect ratio of axial to radial sizes will approach unity [26]. This directly shows that the observed anisotropy is a consequence of interactions.

2.1.2 Low-lying collective modes

The low-lying collective modes are excited as the response of the fermi condensate to the perturbations. A local density perturbation will propagate at the speed of sound, while a global modulation of the trapping potential will

induce a periodic oscillation of the whole fermi cloud.

2.1.2.1 Speed of sound

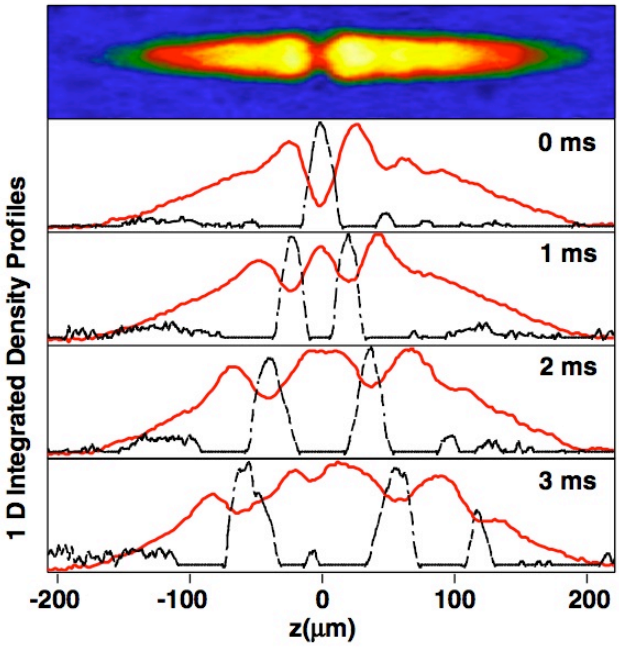

Figure 2.2: Sound propagation in a trapped ultra-cold fermi gas. (Top) The absorption image immediately after being shot by a laser beam into the center. (Bottom) Perturbed density profile (red solid curve) and the difference between the perturbed and unperturbed profiles (black dashed curve) for various propagation times. From [27].

A local density perturbation may be produced by a laser beam focused into the center of the cigar-shaped fermi cloud. The perturbation then propagates along the axial direction of the cloud at the speed of sound c_s. Figure 2.2 shows the propagation of the local density perturbations at different times. The speed of sound also appears in the dispersion relation of collective modes

for uniform systems. The energy of a periodic collective excitation with momentum k is given by $\epsilon_k = c_s k$. Generally, c_s depends on the local density $n(\mathbf{r})$. When the spatial variation of n is small, the speed of sound c_s can be treated spatially-independent as a good approximation, as shown in Figure 2.3.

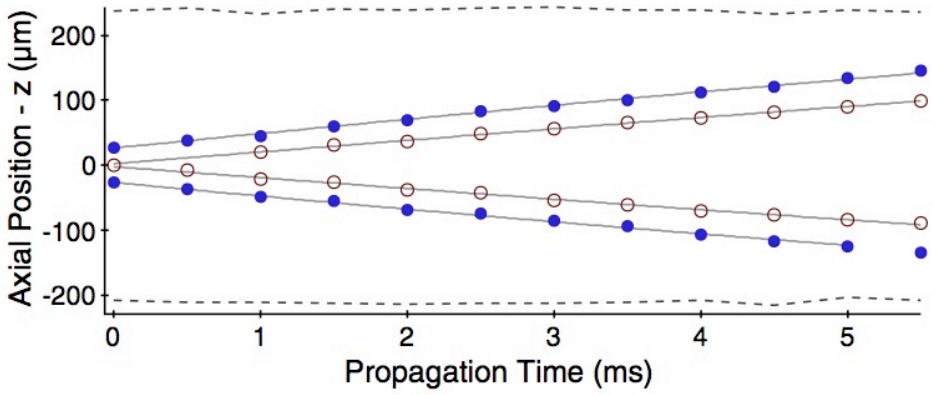

Figure 2.3: The axial propagation of the local density perturbation in the trapped fermi cloud as shown in Figure 2.2. Solid blue circles and open red circles represent the positions of valleys and front peaks, accordingly. From [27].

2.1.2.2 Collective modes for trapped gas

If the confining trap of a fermi condensate is released or changed for a short time interval (for example, 10-ms in [24]), a periodic oscillation of the whole fermi cloud will be induced. Besides the simple sloshing modes that correspond to the center-of-mass oscillations in the trap, the cigar-shaped quantum gas exhibits three elementary, low-lying collective modes: the ax-

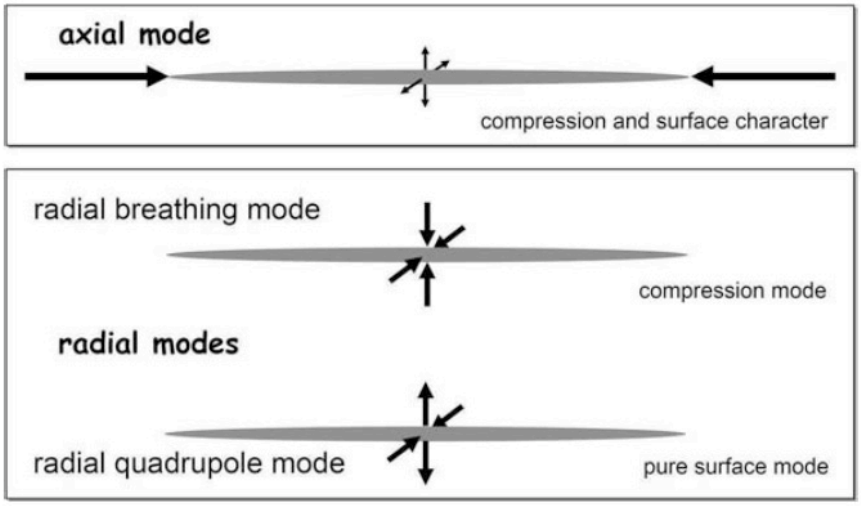

Figure 2.4: The low-lying collective modes of a cigar-like trapped fermi cloud: the axial mode, the radial breathing mode and the radial quadrupole mode, which correspond to the oscillations of the axial size, of the radial radius in phase and of the radial radius 180° out of phase, respectively. From [29].

ial compression mode, the radial breathing mode, and the radial quadrupole mode, as illustrated in Figure 2.4. The axial mode corresponds to a slow oscillation ($\omega \propto \omega_z$) of the axial size of the fermi cloud while the two radial modes correspond to fast oscillations ($\omega \propto \omega_\perp$, and $\omega_\perp \gg \omega_z$ for cigar-shaped quantum gas) at the radial direction. The radial quadrupole mode corresponds to a 180° out of phase oscillation in the x and y direction, while the radial breathing mode corresponds to an in phase oscillation of the radial radius.

2.2 Hydrodynamic equations of motion

Several theoretical models are proposed to explain the dynamical behaviors of fermionic condensates. A Green function approach is proposed to study the collective mode of a uniform gas (speed of sound) as a resonance in the spectrum of the density-density correlation function [30]. The strong interaction between fermions around the feshbach resonance is computed through the ladder diagram scattering or random phase approximation (RPA). The results for a uniform superfluid fermi gas is then extended to include the effect of a harmonic trap [31]. The Green function approach investigates the dynamics of fermi gas from the microscopic level, and the beyond-mean-field effects is taken account of through ladder diagram or RPA. Another model of the fermi gas dynamics, the hydrodynamic equations of motion [26, 28], is a phenomenological model on the macroscopic level. It is based on the assumption that the macroscopic behavior of a neutral superfluid is governed by the Landau equations of irrotational hydrodynamics. At zero temperature, the hydrodynamic equations of superfluids consist of coupled and closed equations for the density and the velocity field. The evolution of the gas is governed by the continuity equation for the local density $n(\mathbf{r},t)$ and the Euler equation (Newton equation) for the velocity field $\mathbf{v}(\mathbf{r},t)$

$$\frac{\partial n(\mathbf{r},t)}{\partial t} = -\nabla\cdot(n(\mathbf{r},t)\mathbf{v}(\mathbf{r},t)) \tag{2.1}$$

$$\frac{d\mathbf{v}(\mathbf{r},t)}{dt} = -\nabla\left(V(\mathbf{r},t)+\mu(n(\mathbf{r},t))+\frac{v^2(\mathbf{r},t)}{2}\right). \tag{2.2}$$

Here $V(\mathbf{r}, t)$ is the external potential (harmonic potential for trapped gas and constant for the uniform fermi gas) and $\mu[n(\mathbf{r})]$ is the local chemical potential, dependent on the local density $n(\mathbf{r})$ through the equation of state of uniform matter. In a uniform system, the chemical potential is defined as

$$\mu[n] = \frac{\partial F[n]}{\partial n} \tag{2.3}$$

with F the internal energy part of the total ground state energy E_g.

The equation of state describing how the local chemical potential $\mu[n(\mathbf{r})]$ is related to $n(\mathbf{r})$ is essential to hydrodynamic theory. It is obtained based on particular microscopic models beyond the hydrodynamic theory. For an weak-interacting uniform fermi gas with equal number of atoms in the two spin species, the equation of state takes the form

$$\mu[n] = \frac{1}{2}(3\pi^2 n)^{2/3} + 4\pi a \frac{n}{2}, \tag{2.4}$$

where the first term is the kinetic energy of a non-interacting fermi gas and the second term is the mean-field approximation of the interaction between fermions. The ignored exchange and correlation effects will become important in the strongly interacting regime (unitary limit) and greatly affect the equation of state.

A further simplification of the equation of state which is often used in the hydrodynamic theory is to assume that the equation of state is polytropic, i.e., $\mu[n] \propto n^{\lambda}$. The polytropic index λ can be obtained as the logarithmic derivative of the chemical potential

$$\lambda = \frac{n}{\mu}\frac{\partial \mu}{\partial n}. \tag{2.5}$$

Hence the equation of state only depends on a single parameter, the polytropic index λ. λ was calculated from the microscopic mean field description introduced by A. Leggett [32]. The calculated dependence of λ in the BEC-BCS crossover is shown as the solid line in Figure 2.5 as a function of $1/k_F a$. The polytropic index $\lambda = 1$ in the BEC limit, which coincides with the known equation of state $\mu = Vn$. The index then decreases across the unitary limit to a minimum value of about $\lambda = 0.6$ at $1/k_F a \approx -0.5$ before it subsequently increases to $\lambda = 2/3$ in the BCS limit, as expected from (2.4) when the interaction constant is small. At the unitary limit the index $\lambda = 2/3$ is the same as that of BCS limit.

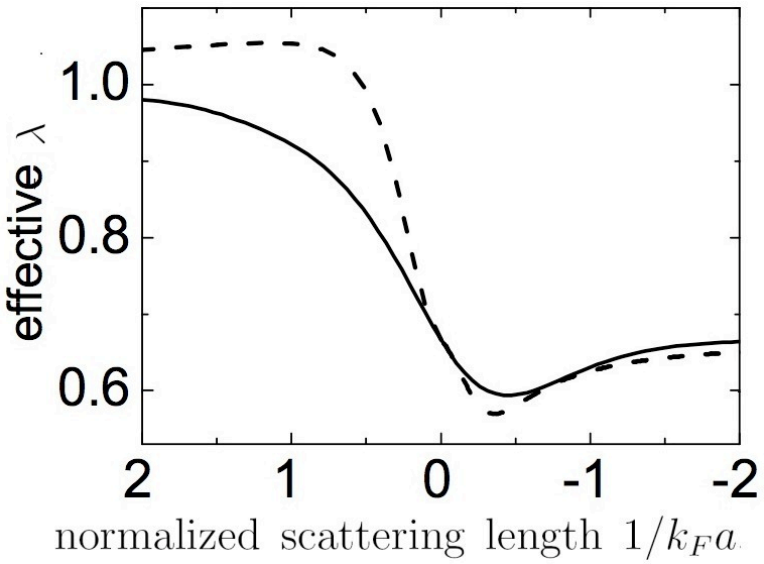

Figure 2.5: The polytropic index λ versus the interaction parameter $1/k_F a$ in the BEC-BCS crossover. The solid line represents the mean field approximation [32]. The dashed line is from the results of a Monte Carlo calculation [33]. From the inset of Figure 3.10 of [34].

As we mentioned above, at the unitary limit, the ignored exchange and correlation effects become important and the mean-field approximation is not sufficient for the equation of state. More sophisticated approaches are proposed to include the beyond-mean-field effects using diagrammatic techniques [35, 36, 37]. But still, these theories are only qualitatively correct in the unitary limit. The Quantum Monte Carlo techniques [33], which are based on numerical simulations, are believed to be the most accurate approach in dealing with strongly correlated systems and are applied to calculate the equation of state (dashed line in Figure 2.5). In contrary to the monotonic decrease from the BEC limit to the unitary limit predicated by the mean field approximation, the index λ first increases to values larger than 1 before it decreases to $\lambda = 2/3$ at the unitary limit. It is worthy to notice that the values of index λ are the same for the three limits: $\lambda = 1$ at BEC-limit, $\lambda = 2/3$ at BCS limit and $\lambda = 2/3$ at the unitary limit.

Based on the data obtained from the Quantum Monte Carlo calculations, an analytical fitting formula for the equation of state of a uniform two-component fermi gas is proposed in [38]. At zero temperature, the internal energy F is written as

$$F = \frac{3}{5} n \epsilon_F \epsilon(y), \tag{2.6}$$

where $\epsilon_F = k_F^2/2$ is the fermi energy for non-interacting fermi gas and $\epsilon(y)$ is a yet unknown function of the interaction parameter $y = 1/(k_F a)$. It is

	BCS ($y<0$)		BEC ($y>0$)	
	Expression	Value	Expression	Value
α_1	ξ	0.4200	ξ	0.4200
α_2	$\frac{2}{\pi}(1-\alpha_1)$	0.3692	$\frac{2}{\pi}\alpha_1$	0.2674
α_3	$\frac{9\pi}{10}\alpha_2$	1.0440	$\frac{18\pi}{5}\alpha_2\frac{a_M}{a}$	5.0400
β_1	[fitted]	1.4328	[fitted]	0.1126
β_2	$\alpha_2\alpha_3\beta_1/\zeta_-$	0.5523	$\alpha_2\alpha_3\beta_1/\zeta_+$	0.4552

Figure 2.6: Parameters of the fitting function (2.7), as given in [38]

suggested [38] that the analytical fitting formula takes the form

$$\epsilon(y) = \alpha_1 - \alpha_2 \arctan\left(\alpha_3 y \frac{\beta_1 + |y|}{\beta_2 + |y|}\right), \tag{2.7}$$

which interpolates the Monte Carlo data and asymptotic behaviors of $y = 1/(k_F a)$. Two sets of fitting parameters are obtained, one set in the BCS region ($x < 0$) and a separate set in the BEC region ($x > 0$). The fitting values of these parameters are reported in Figure 2.6, and the fitting curve is presented in Figure 2.7. An analytical functional parameterization of $\epsilon(y)$ allows straightforward analytical calculations of the equation of state

$$\mu = \frac{\partial F}{\partial n} = \epsilon_F \left(\epsilon(y) - \frac{y}{5}\epsilon'(y)\right). \tag{2.8}$$

With the availability of the equation of state explicitly expressed as function of density n, either from the analytical fitting of the Monte Carlo data [33] or from the mean-field approximation [32], the hydrodynamic equations of

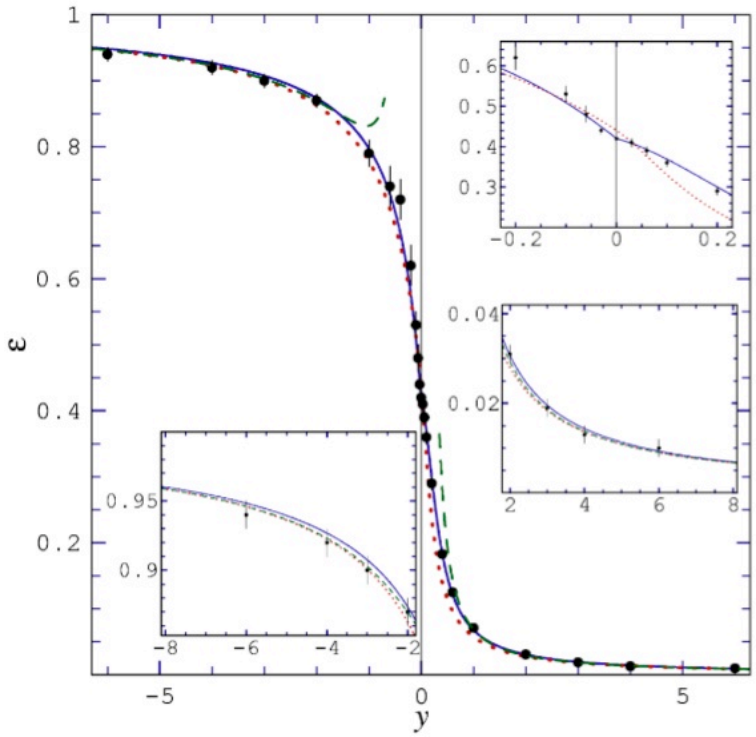

Figure 2.7: The fitting curve of the particle energy $\epsilon(y)$ (the solid line) according to the formula given by (2.7) and the fixed-node Monte Carlo data points [33](solid circles). The parameters of the fitting curve are listed in Figure 2.6. From [38].

motion (2.2) are now ready to be put to use. I will briefly review its application to explain the experimental data in these two aspects, anisotropic expansion, collective modes for trapped gas and the speed of sound.

2.2.1 Anisotropic expansion

In the case of free expansion, the external potential term $V(\mathbf{r}, t)$ in the hydrodynamic equations of motion (2.2) is a piecewise function. $V(\mathbf{r}, t)$ is

equal to the initial harmonic trapping potential

$$V(\mathbf{r}) = \frac{1}{2}\left(\omega_z^2 z^2 + \omega_\perp^2 (x^2 + y^2)\right), \tag{2.9}$$

for $t < 0$ and equal to zero for $t > 0$. The polytropic assumption of the equation of state, together with the local density approximation (LDA), allows the analytic form of local density

$$n(\mathbf{r}) \propto (\mu_0 - V(\mathbf{r}, t))^{1/\lambda} \tag{2.10}$$

It was found [39] that the hydrodynamic equations of motion have a simple scaling solution

$$n(x, y, z, t) = (b_x b_y b_z)^{-1} n_0 \left(\frac{x}{b_x}, \frac{y}{b_y}, \frac{z}{b_z}\right) \tag{2.11}$$

with the scaling parameters $b_i(t)$ obeying [29]

$$\ddot{b}_i = -\omega_i^2(t) b_i + \frac{\omega_i^2(0)}{b_i (b_x b_y b_z)^\lambda}. \tag{2.12}$$

The equation of motion for the scaling parameters $b_i(t)$ only depends on the polytropic index λ, and can be solved numerically with initial conditions $b_i(0) = 1$ and $\dot{b}_i(0) = 0$.

Compared with the experimental data of a free expansion of an ultracold fermi cloud shown in Figure 2.1, the predictions for the aspect ratio based on the hydrodynamic theory (2.12) are shown in Figure 2.8. The experiment is conducted in the regime of strongly attractive interaction with $a \sim -10^4 a_0$ (a_0 is the scattering length without Feshbach resonance), which is close to the

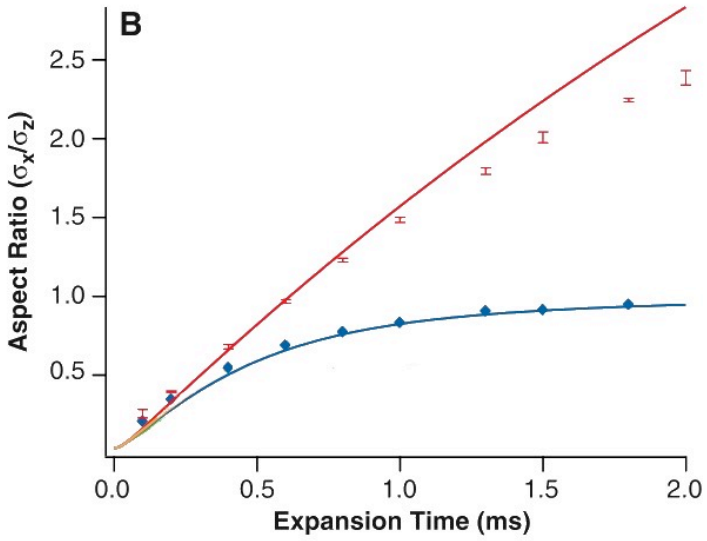

Figure 2.8: The time evolution of the aspect ratio of a freely-expanding fermi cloud after released from the confining trap. At unitary limit: error bars $\sim$ experiment; red (upper) curve $\sim$ hydrodynamic theory with $\lambda = 2/3$. In the absence of interactions: diamonds $\sim$ experiment; blue (lower) curve $\sim$ ballistic expansion. From [23].

unitary limit with the polytropic index $\lambda = 2/3$. The aspect ratio is defined as

$$\frac{\sigma_x}{\sigma_z} = \frac{\omega_z}{\omega_\perp}\frac{b_x(t)}{b_z(t)}, \tag{2.13}$$

where $\omega_z/\omega_\perp = 0.035$ is the initial aspect ratio [23].

The inversion of the aspect ratio is a consequence of the interaction between fermions, as illustrated in Figure 2.8. For ideal non-interacting fermi gases, the density profile after free expansion should have the same form as that before the trap is switched off, but with scaling parameter $b_i(t) = \sqrt{1+\omega_i^2 t^2}$

[29]. For a cigar-shaped fermi cloud, the radial size where the original confining trap is stronger has a larger increasing speed. However, for the non-interacting fermi gases, the aspect ratio will not be inverted but with the final aspect ratio approaching 1,

$$\frac{\sigma_x}{\sigma_z} = \frac{\omega_z}{\omega_\perp}\frac{\sqrt{1+\omega_x^2 t^2}}{\sqrt{1+\omega_z^2 t^2}} \to 1, \quad \text{as} \quad t \to \infty. \tag{2.14}$$

2.2.2 Low-lying collective modes

Collective modes are the solutions of the hydrodynamic equations for the geometry of the external potential applied. Let us consider small perturbations of the density $n = n_0 + \delta n \exp(-i\omega t)$ and velocity $\mathbf{v} = \delta\mathbf{v}\exp(-i\omega t)$, with respect to the equilibrium state with density $n_0(\mathbf{r})$ and zero velocity. The linearized hydrodynamic equations of motion up to the first order takes the form:

$$-\omega^2 \delta n = \nabla \cdot \left[n_0 \nabla \left(\frac{\partial \mu}{\partial n} \delta n \right) \right]. \tag{2.15}$$

2.2.2.1 Collective mode for trapped gas

In the presence of axisymmetric harmonic potential (2.9), the local density profile n_0 is given by (2.10) based on the assumptions of polytropic equation of state and LDA. The lowest energy solutions of (2.15) are discretized, with the energy ω being the order of the trapping frequencies. Several low-lying collective modes [40] of the trapped gas have been observed experimentally [29].

- The dipole mode (sloshing mode) is the overall movement of the whole fermi cloud as a single entity with no change in the internal structure. Thus it is independent of the internal interactions since these interactions depend only on the relative distances between fermions which are kept constant in this mode. The dipole mode corresponds to a center of mass oscillation with frequency $\omega = \omega_\perp$ when $\delta n \propto x \pm iy$ and $\omega = \omega_z$ when $\delta n \propto z$.

- The radial quadrupole mode, with a density perturbation $\delta n \propto (x \pm iy)^2$, is a pure surface mode where a 180° out of phase sharp deformation oscillates on the radial direction without any change of the volume. Its frequency

$$\omega = \sqrt{2}\omega_\perp \tag{2.16}$$

  is independent of the equation of state and do not change across the BEC-BCS crossover, as long as the system is hydrodynamic.

- The radial breathing mode is a compression mode where the density perturbation

$$\delta n \propto a + b(x^2 + y^2) + cz^2 \tag{2.17}$$

  is independent of the inclination and azimuth angles. For elongated traps, where $\omega_z \ll \omega_\perp$, the linearized equation of motion (2.15) has two nontrivial solutions. One is

$$\omega = \sqrt{2\lambda + 2}\,\omega_\perp \tag{2.18}$$

for the radial breathing mode, and the other solution is called the axial mode.

- The axial mode is an oscillation of the length of the cigar shape gas with the frequency

$$\omega = \sqrt{\frac{3\lambda + 2}{\lambda + 1}}\, \omega_z. \tag{2.19}$$

The compression modes depend on the compressibility of the gas, so both the radial breathing mode and the axial mode rely on the polytropic index λ of the equation of state, and thus they will vary accordingly by tuning the interactions along the BEC-BCS crossover.

		Hydrodynamic		Collisionless, non-superfluid
		mBEC $(1/k_{\mathrm{F}}a \gg 1)$	unitarity $(1/k_{\mathrm{F}}a = 0)$	
Axial mode	$\omega_{\mathrm{ax}}/\omega_z$	$\sqrt{5/2} = 1.581..$	$\sqrt{12/5} = 1.549..$	2
Radial compression mode	$\omega_{\mathrm{c}}/\omega_{\mathrm{r}}$	2	$\sqrt{10/3} = 1.826..$	2
Radial quadrupole mode	$\omega_{\mathrm{q}}/\omega_{\mathrm{r}}$	$\sqrt{2} = 1.414..$	$\sqrt{2} = 1.414..$	2

Figure 2.9: Oscillating frequencies for the collective modes in different regimes. From [29]

An overview of the frequencies of the three low-lying modes are presented in Figure 2.9. The critical temperature T_c for superfluid phase transition at the BCS limit, where $T_c \propto \epsilon_F e^{\frac{\pi}{2k_F a}}$, is much lower than that at the BEC limit and unitary limit, where the T_c is in the same order of the Fermi temperature T_F (Figure 2.10). The Fermi temperature $T_F = \frac{\hbar^2}{2mk_B} n^{2/3}$ is around

or below one μK for typical experimental conditions. In Figure 2.9, a collisionless, non-superfluid regime is listed instead of the BCS limit, because a superfluid state of matter is not achieved when the interaction is tuned to the regime $k_F a \ll -1$ for the temperature in current experiments. Furthermore, the Pauli blocking effect greatly suppresses the fermion collisions and the ultracold fermi gas become collisionless and non-interacting. In the absence of interactions, the oscillation frequency ω is the same as that for single fermion in the presence of a harmonic potential, $\omega = l\omega_i$ with $i = z, \perp$ and l is an integer. In this case, the oscillation frequency for ideal fermi gas are integer multiples of the trap frequency.

The frequency of the radial compression mode is measured [42] in a strongly interacting, optically trapped Fermi gas of ^{6} Li atoms. A relative accuracy level of 10^{-3} is achieved with better control of the ultra-cold superfluid system. The precision measurements, compared with theoretical prediction of hydrodynamic equations of motion, is presented in Figure 2.11 along the BEC-BCS crossover. The equation of state $\mu[n]$ is obtained with either the Quantum Monte Carlo calculation (2.8) (upper curve) or the mean-field approximation (2.4) (lower curve). Because of the low uncertainties, it is clear to see that the experimental data fits better with the quantum Monte Carlo data. It also shows the presence of the beyond-mean-field effects in the strongly interacting BEC side, which shift the normalized frequency up.

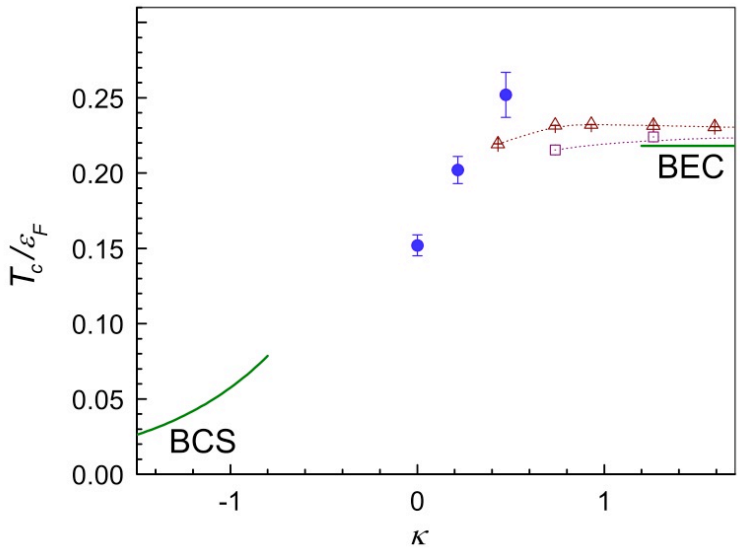

Figure 2.10: The critical temperature for superfluid phase transition versus the interaction parameter $\kappa = 1/k_F a$ in the BEC-BCS crossover. The solid line shows the theoretical predictions based on mean-field approximation at both the BEC and BCS limits. The three solid circles are obtained by the Monte Carlo calculation. From [41].

2.2.2.2 Speed of sound

In a uniform system where the density n_0 is spatial independent, we have from (2.15) that

$$-\omega^2 \delta n = n_0 \frac{\partial \mu}{\partial n} \nabla^2 (\delta n) = \lambda \mu \nabla^2 (\delta n) , \tag{2.20}$$

where the assumption of the polytropic equation of state is applied in the deviation. The solutions of (2.20) correspond to sound waves with dispersion relation

$$\omega = \sqrt{\lambda \mu}\, q. \tag{2.21}$$

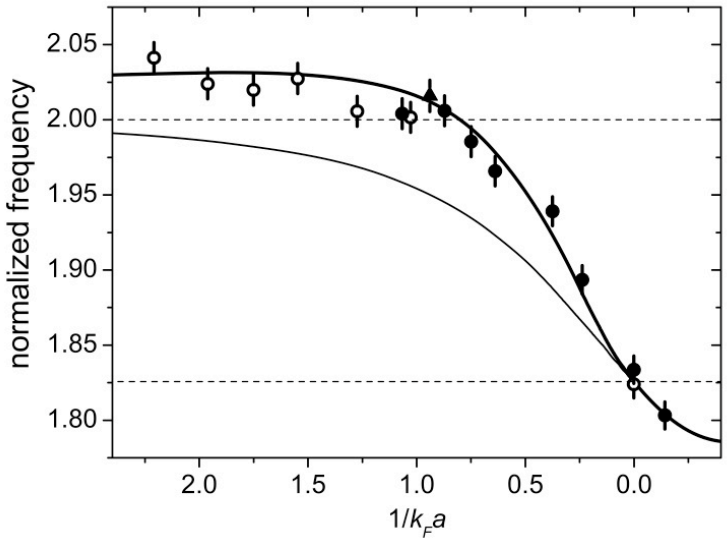

Figure 2.11: The theoretical calculations and experimental measurements of the radial breathing mode frequency. The upper curve corresponds to the Quantum Monte Carlo calculations [33] and the lower curve refers to the mean-field BCS theory [32]. Theoretical values for the BEC limit $\omega = 2\omega_\perp$ and the unitary limit $\omega = \sqrt{10/3}\omega_\perp$ are indicated by the upper and lower horizontal dashed lines accordingly. From [42].

- In the BEC limit, where $\lambda = 1$ and the chemical potential $\mu = Vn$, one recovers the Bogoliubov result $c = \sqrt{Vn}$ for the sound velocity.

- In the BCS limit, where $\lambda = 2/3$ and the chemical potential $\mu = \frac{1}{2}(3\pi^2 n)^{2/3} + \frac{1}{2}Vn$, the speed of sound $c = \frac{v_F}{\sqrt{3}}\sqrt{1 + \frac{4k_F a}{3\pi}}$, the same as expected from the Bogoliubov-Anderson mode.

- At the unitary limit, where $\lambda = 2/3$ and $\mu = (1+\beta)\epsilon_F$, one has the result $c = (1+\beta)^{1/2} v_F/\sqrt{3}$.

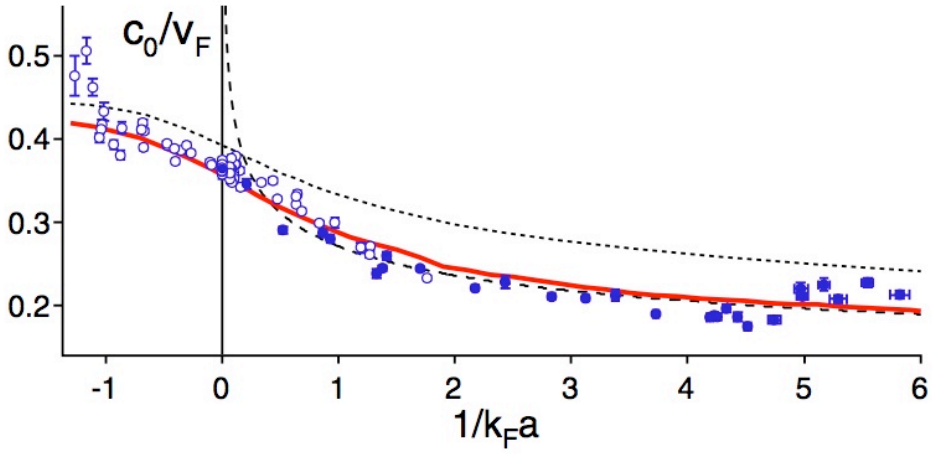

Figure 2.12: Normalized sound velocity c_0/v_F predicted by the hydrodynamic theory with the equation of state given by three different approaches: 1. mean-field theory based on Leggett [32] (black dotted curve); Quantum Monte Carlo calculation [33] (gray solid curve); Thomas-Fermi theory of a molecular BEC, using $a_{mol} = 0.6a$ (black dashed curve). From [27].

When a local density perturbation is induced at the center of a fermi cloud, it will propagate with the speed of sound. As we can see above, the speed of sound depends on the local density $n(\mathbf{r})$, therefore the propagation of sound will be affected by the inhomogeneity of the trapped fermi cloud. However, when the spatial variation of density profile is slow, it is good enough to consider the speed of sound as constant within a certain spatial extent. The speed of sound is measured in the trapped fermi gas [27] throughout the crossover region, from a weakly interacting Fermi gas through the resonant Fermi superfluid regime to a Bose condensate of dimer molecules. The experimental data is then compared with the prediction of hydrodynamic theory, as

illustrated in Figure 2.12. The same as that for the trapped gas, the measurements of speed of sound fits better with the Monte Carlo equation of motion, compared to the mean field approximation.

2.3 Advantage and limitation of hydrodynamic theory

Compared to other dynamical models of BEC-BCS crossover, the hydrodynamic theory has several advantages: it is more intuitive; it can be easily applied to include a confining trap; the low-lying collective modes of a harmonically trapped fermionic superfluid can be analytically studied; it can be directly adopted to study the anisotropic expansion; and most importantly, to a satisfactory extent, it matches well with the experimental data.

However, the hydrodynamic theory also has several limitations, as listed below:

First, it is a phenomenological model and a solid microscopic foundation is missing. After the experimental realization of BEC [3] in 1995, a time-dependent Gross-Pitaevskii (GP) equation was proposed to describe the dynamics of weakly interacting bose gases

$$i\hbar\frac{\partial}{\partial t}\psi(\mathbf{r},t) = \left(-\frac{\hbar^2}{2m}\nabla^2 + V(\mathbf{r},t) + \mu(n(\mathbf{r},t))\right)\psi(\mathbf{r},t). \tag{2.22}$$

This mean-field theory has proven capable to provide a satisfactory description of the experimental data in the weak-interacting BEC regime [23]. If we rewrite the complex order parameter $\psi(\mathbf{r},t) = \sqrt{n(\mathbf{r},t)}\exp[i\phi(\mathbf{r},t)]$ in terms of the superfluid density $n(\mathbf{r},t)$ and velocity $v(\mathbf{r},t) = \nabla\phi(\mathbf{r},t)$ as gradient

of the phase, we will get the hydrodynamic equations of motion (2.2) for classical irrotational flow. In other words, the hydrodynamic equations of motion are an alternative expression of the mean-field GP equation whose validity is restricted to the BEC limit.

In the BCS side, an equation whose structure is similar to GP equation is the Ginzburg-Landau equation, which is however valid only close to the critical temperature T_c where the order parameter is sufficiently small. It is then unclear that why the classical hydrodynamic theory, which was derived as an alternative expression of the mean-field GP equation in the BEC limit, is able to successfully describe dynamics of the highly quantum fermi condensate along the whole BEC-BCS region and beyond the mean-field approximation.

Second, the hydrodynamic theory is limited to the local density approximation (LDA). $\mu(n(\mathbf{r}))$ appearing in the hydrodynamics equations of motion (2.2) is the local chemical potential fixed by the equation of state of a uniform matter. The applicability of the LDA has proven to be adequate to describe fermionic superfluids with equal number of atoms occupying two different spin states. However, some recent experiments are conducted in more complex systems where the number of atoms in the two spin states is different, i.e., $n_\uparrow \neq n_\downarrow$[43, 44, 45]. It is demonstrated in Figure 2.13 that the experimental data differs by a factor of 10 from expectation of LDA.

Therefore, we hope to systematically develop a general formalism for the dynamics of BEC-BCS crossover which bypasses LDA. Yet we would still like to adopt the adiabatic assumption so that the dynamics of the quantum

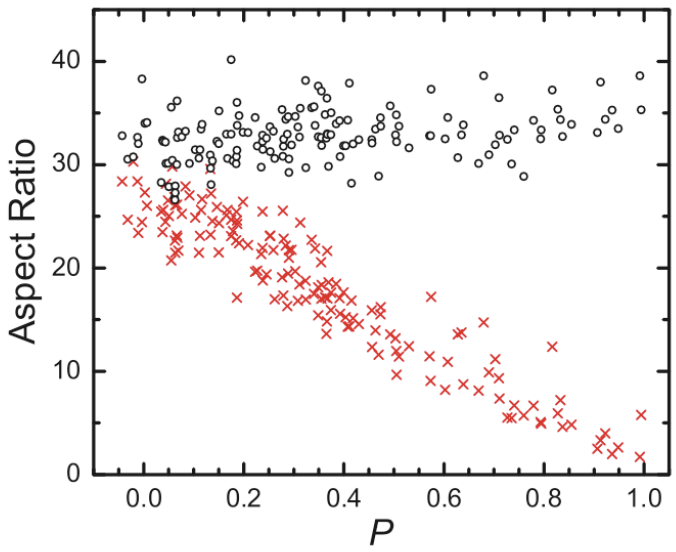

Figure 2.13: Aspect ratio vs $P = (N_\uparrow - N_\downarrow)/(N_\uparrow + N_\downarrow)$. The ratio of the axial to the radial dimensions of the confined fermi gas, is shown for the majority state $|1\rangle$ by the black circles and for the minority state $|2\rangle$ by the red crosses. As the aspect ratio of $|1\rangle$ is close to the theoretical prediction based LDA, the aspect ratio of $|2\rangle$ differs by a factor of 10. From [45]

system can be investigated practically compared to those exact theoretical modes like time-dependent DFT.

My results will be presented in the next three chapters. In chapter 3, I will develop a static density functional theory specially formalized for the spin-polarized superfluid. The density functional theory is exact without any spatial approximation such as the local density approximation. In chapter 4, a general formalism for the adiabatic dynamics in the BEC-BCS crossover is derived based on the static DFT of chapter 3. The adiabatic equations of motion

are exact in the adiabatic limit. To study the normal modes for experimental interests, the adiabatic equations of motion are further linearized based on the small amplitude approximation. The adiabatic dynamic theory is obtained after a rigorous derivation, but we still want to check what it is like under special conditions. In chapter 5, we show that our adiabatic equations of motion are reduced to the hydrodynamic equations of motion within local density approximation. This serves as a verification of the adiabatic dynamic theory, and also provides a solid microscopic foundation for the phenomenological hydrodynamic theory. A conclusion is given in chapter 6.

Chapter 3

DFT for Spin-Polarized Superfluids

In this chapter, we develop a density-functional theory for spin-polarized superfluids, which is a generalization of the density-functional theory for superconductors [46] to include the spin-polarization effects for current experimental interests. This static density-functional theory also serves as a foundation of the adiabatic dynamics theory we develop to study the low-lying collective modes in the BEC-BCS crossover. The adiabatic dynamics theory will be discussed with details in the next chapter.

3.1 Density functional theory

Density-functional theory (DFT)[47, 48, 49, 50, 51] works as a powerful tool to investigate the properties of many-body systems with a very large number (N) of particles involved. The many-body wavefunction $\Psi_0(\cdots, \mathbf{r}_i\sigma_i, \cdots)$ for these particles contains a great deal of information, and any observable $\hat{O}$ can be computed as the expectation value $\langle\Psi_0|\hat{O}|\Psi_0\rangle$ in the ground state. However, it is technically impossible to compute the wavefunction by solving the corresponding Schrodinger equation, or store it with required accuracy since it is a function of $3N$ variables. DFT told us that the density, $n(\mathbf{r})$, which

is a function of only three coordinates, contains all the information we would need for the ground state of the many body system.

The DFT is built on two theorems proved by Kohn and Hohenberg [47]. The first one says that all the ground state properties, including the ground state energy E_g and wave function Ψ_0, are uniquely determined by the ground state density $n(\mathbf{r})$. The second theorem describes the way how $n(\mathbf{r})$ can be calculated through a variational principle: the ground state energy is minimized by the true ground state density. If the form of the ground state energy as a functional of the density is known, we could simply vary the density until the energy is minimized, which directly gives us the ground state density and therefore all the ground state properties. However, the explicit expression of ground state energy dependent on $n(\mathbf{r})$ is unknown in most of the cases. An equivalent yet more practical approach to calculate $n(\mathbf{r})$ was proposed by Kohn and Sham [48], who showed that $n(\mathbf{r})$ of an interacting system could be produced by solving a corresponding fictitious non-interacting system which has the same ground state density. As the particles in the fictitious system are non-interacting, $n(\mathbf{r})$ can be obtained by calculating the eigenfunctions $\psi_i(\mathbf{r})$ and eigenvalues ϵ_i of the single-particle and self-consistent Kohn-Sham equations

$$\left(-\frac{1}{2}\nabla^2 + v_s(\mathbf{r})\right)\psi_i(\mathbf{r}) = \epsilon_i\psi_i(\mathbf{r}) \tag{3.1}$$

with

$$n(\mathbf{r}) = \sum_{1}^{N} |\psi_i(\mathbf{r})|^2. \tag{3.2}$$

The effective potential $v_s(\mathbf{r})$, which is completely determined for a given density distribution, consists of three parts

$$v_s(\mathbf{r}) = v_{ext}(\mathbf{r}) + v_{MF}(\mathbf{r}) + v_{xc}(\mathbf{r}), \tag{3.3}$$

an external part $v_{ext}(\mathbf{r})$, a mean-field approximation part $v_{MF}(\mathbf{r})$ and an exchange-correlation part (xc) $v_{xc}(\mathbf{r})$ which represents the many-body effects of the original interacting system. The xc potential is the only term not explicitly given in the Kohn-Sham equations, an approximation based on specific models is needed in its description.

With the ground state density self-consistently computed from the Kohn-Sham equations (3.1) and (3.2), all the properties of the ground state, in particular the ground state energy, becomes available [51]

$$E_g[n(\mathbf{r})] = T_s + \int d\mathbf{r} v_{\mathrm{ext}}(\mathbf{r}) n(\mathbf{r}) + \frac{1}{2} \int d\mathbf{r} v_{\mathrm{MF}}(\mathbf{r}) n(\mathbf{r}) + F_{xc}[n(\mathbf{r})] \tag{3.4}$$

with $T_s = \langle \Psi_{\mathrm{KS}} | \hat{T} | \Psi_{\mathrm{KS}} \rangle$ the kinetic energy of the non-interacting Kohn-Sham system. $F_{xc}[n(\mathbf{r}]$ is the exchange-correlation energy which is related to $v_{xc}(\mathbf{r})$ by $v_{xc}(\mathbf{r}) = \partial F_{xc}[n(\mathbf{r})]/\partial n(\mathbf{r})$.

3.2 DFT for ordered states

When the symmetry of a system is broken, one or more extra variables are needed to describe the new ordered state of the system. These variables, which are called order parameters, should also be included as basic variables in description of the ordered states such as magnetic materials and superfluids.

- Spin-density functional theory (spin-DFT) for magnetic materials[52, 53, 54]: In magnetic materials, the spatial rotation symmetry is spontaneously broken with the order parameter, the magnetization density $\mathbf{m}(\mathbf{r})$ pointing to a certain direction. In the interests of this dissertation, it is sufficient to consider the component of the magnetization along a fixed direction, the spin polarization $m(\mathbf{r}) = n_\uparrow(\mathbf{r}) - n_\downarrow(\mathbf{r})$. This corresponds physically to the coupling of the particle spin to an external magnetic field which has only one non-zero component. It is also convenient to switch from $n(\mathbf{r})$ and $m(\mathbf{r})$ to the spin densities $n_\uparrow(\mathbf{r})$ and $n_\downarrow(\mathbf{r})$ as fundamental variables to describe systems in which the external fields $v_\uparrow(\mathbf{r})$ and $v_\downarrow(\mathbf{r})$ are different for each of the two spin components . A one-to-one mapping can be established between the particle densities $n_\uparrow(\mathbf{r})$ and $n_\downarrow(\mathbf{r})$ and external potentials $v_\uparrow(\mathbf{r})$ and $v_\downarrow(\mathbf{r})$, and all other quantities of ground state can be regarded as functionals of the two spin densities.

  The Kohn-Sham equations with spin polarization become

$$\left(-\frac{1}{2}\nabla^2 + v_{s\alpha}(\mathbf{r})\right)\psi_{i\alpha}(\mathbf{r}) = \epsilon_{i\alpha}\psi_{i\alpha}(\mathbf{r}) \tag{3.5}$$

  with

$$n_\alpha(\mathbf{r}) = \sum_1^N |\psi_{i\alpha}(\mathbf{r})|^2, \quad \alpha = \uparrow, \downarrow . \tag{3.6}$$

  The equations (3.5) and (3.6) serve as the basic equations for the DFT of magnetic materials. This spin-DFT would be reduced to the regular DFT if the system is spin-unpolarized.

- Density functional theory for the superfluid state of matter (DFT for superfluids) [46, 55]: In superfluids , the order parameter which breaks the gauge symmetry is the complex anomalous density

$$d(\mathbf{r}, \mathbf{r}') = \langle \psi_\uparrow(\mathbf{r}) \psi_\downarrow(\mathbf{r}') \rangle \tag{3.7}$$

where $\psi_\alpha(\mathbf{r})$ is the field operator for spin α at position $\mathbf{r}$. The DFT for superfluids ensures that the superfluid systems can be described completely and, in principle, exactly in terms of $n(\mathbf{r})$ and $d(\mathbf{r}, \mathbf{r}')$. Again in the interests of this dissertation, we assume that the interactions between particles are local for simplicity. A generalization to non-local interactions poses no significant problems. As a direct consequence of the local interaction, only the diagonal terms of the anomalous density $d(\mathbf{r}) \equiv d(\mathbf{r}, \mathbf{r})$ survive.

The Kohn-Sham equations in DFT for superfluids are a generalization of the mean-field Bogoliubov-de Gennes (BdG) equations, namely

$$\begin{pmatrix} \hat{h}(\mathbf{r}) & D_s(\mathbf{r}) \\ D_s^*(\mathbf{r}) & -\hat{h}(\mathbf{r}) \end{pmatrix} \begin{pmatrix} u_m(\mathbf{r}) \\ v_m(\mathbf{r}) \end{pmatrix} = \epsilon_m \begin{pmatrix} u_m(\mathbf{r}) \\ v_m(\mathbf{r}) \end{pmatrix} \tag{3.8}$$

with the particle density

$$n(\mathbf{r}) = 2 \sum_m \left[|u_m(\mathbf{r})|^2 \Theta(-\epsilon_m) + |v_m(\mathbf{r})|^2 \Theta(\epsilon_m) \right] \tag{3.9}$$

and complex anomalous density

$$d(\mathbf{r}) = \sum_m v_m^*(\mathbf{r}) u_m(\mathbf{r}) \left(\Theta(\epsilon_m) - \Theta(-\epsilon_m) \right). \tag{3.10}$$

Here $\hat{h} = -\nabla^2/2 - \mu + v_s(\mathbf{r})$ is the single-particle Hamiltonian, $\Theta(x)$ the heaviside step function, $v_s(\mathbf{r})$ and $D_s(\mathbf{r})$ are the effective particle potential and pair potential which are coupled to $n(\mathbf{r})$ and $d(\mathbf{r})$, respectively.

3.3 DFT for spin-polarized superfluids

For the system of spin-polarized superfluids, there are two finite order parameters appearing in addition to the particle density: the spin polarization density $m(\mathbf{r})$ and the complex anomalous density $d(\mathbf{r})$. Thus, the system can be completely described in terms of four real fields, $n(\mathbf{r})$, $m(\mathbf{r})$ and the real and imaginary parts of $d(\mathbf{r})$. (Please refer to the Appendix A for a brief proof.) In the following section, I will develop a DFT specially formalized for spin-polarized superfluids. The central results are a set of self-consistent equations by solving which one can in principle obtain the four basic variables and all the ground state properties exactly. In the first part, we write the Kohn-Sham equations for the fictitious non-interacting particles. In the second part, we show that the Kohn-Sham equations can be simplified by using particle-hole symmetry, and the final results may be regarded as a generalization of the BdG equations for normal superfluids (3.8) to include the spin polarization effects.

3.3.1 General formalism

Instead of the four basic variables, $n(\mathbf{r})$, $m(\mathbf{r})$, $d_R(\mathbf{r})$ and $d_I(\mathbf{r})$, alternatively a set of four general densities $\rho_i(\mathbf{r})$ can be used, which are defined

as

$$\rho_i = \langle\Psi_0|\hat{\rho}_i|\Psi_0\rangle = \langle\Psi_0|\Phi^\dagger(\mathbf{r})\tau_i\Phi(\mathbf{r})|\Psi_0\rangle \tag{3.11}$$

with the Nambu particle-hole spinor [56, 57] $\Phi^\dagger(\mathbf{r}) = \left(\psi^\dagger_\uparrow(\mathbf{r}), \psi_\downarrow(\mathbf{r})\right)$. The four matrices τ_i are the 2×2 unit matrix $\mathbf{1}$ for $i = 0$ and the Pauli spin matrices for $i = 1, 2, 3$. The connection between $n(\mathbf{r})$, $m(\mathbf{r})$, $d(\mathbf{r})$ and $\rho_i(\mathbf{r})$ is given by

$$\begin{aligned}
\rho_0(\mathbf{r}) &= m(\mathbf{r}) && (3.12)\\
\rho_1(\mathbf{r}) &= -d(\mathbf{r}) - d^*(\mathbf{r}) = -2d_R(\mathbf{r}) && (3.13)\\
\rho_2(\mathbf{r}) &= -id(\mathbf{r}) + id^*(\mathbf{r}) = 2d_I(\mathbf{r}) && (3.14)\\
\rho_3(\mathbf{r}) &= n(\mathbf{r}). && (3.15)
\end{aligned}$$

In other words, the basic variables, $n(\mathbf{r})$, $m(\mathbf{r})$, $d_R(\mathbf{r})$ and $d_I(\mathbf{r})$, can be closely related through the general densities in a very compact and integrated way. In the rest part of this dissertation, I will alternatively use these two sets of variables: the basic variables possess more direct physical meanings while the general densities would greatly simplify the mathematical expressions.

Consider a superfluid system described by a grand-canonical Hamiltonian in the following form (atomic units are used throughout this dissertation)

$$\hat{H} = \hat{T} + \hat{U} + \hat{W}, \tag{3.16}$$

which consist of three parts: a spin-dependent kinetic energy

$$\hat{T} = \sum_\alpha \int d\mathbf{r}\ \psi^\dagger_\alpha(\mathbf{r}) \left(-\frac{\nabla^2}{2m_\alpha}\right) \psi_\alpha(\mathbf{r}), \tag{3.17}$$

where the mass of atoms in the two spin states is different ($m_\uparrow \neq m_\downarrow$) for experimental interests; a local particle-particle interaction

$$\hat{U} = V \int d\mathbf{r}\ \psi_\uparrow^\dagger(\mathbf{r})\psi_\downarrow^\dagger(\mathbf{r})\psi_\downarrow(\mathbf{r})\psi_\uparrow(\mathbf{r}) \tag{3.18}$$

with the $V = 4\pi a$ characterized by the s-wave scattering length a; and the external potentials coupled to all the four general densities

$$\hat{W} = \sum_i \int d\mathbf{r}\hat{\rho}_i(\mathbf{r})W_i(\mathbf{r}). \tag{3.19}$$

Here, $W_3(\mathbf{r})$ is the normal potential, $W_1(\mathbf{r}) - iW_2(\mathbf{r})$ represents the complex pair potential coupled to the anomalous density $d(\mathbf{r})$, and $W_0(\mathbf{r})$ describes a Zeeman field coupled to the spin polarization density.

The ground-state energy, as well as the other observables of ground state, can be completely described by the general densities $\rho_i(\mathbf{r})$ and takes the form

$$E_g[\rho_i(\mathbf{r})] = F[\rho_i(\mathbf{r})] + \sum_i W_i(\mathbf{r})\rho_i(\mathbf{r}). \tag{3.20}$$

The internal energy $F[\rho_i(\mathbf{r})]$, as a universal functional of $\rho_i(\mathbf{r})$, can be written in three parts

$$F[\rho_i(\mathbf{r})] = \langle\Psi_0|\hat{T} + \hat{U}|\Psi_0\rangle = T_s[\rho_i(\mathbf{r})] + U_{MF}[\rho_i(\mathbf{r})] + F_{xc}[\rho_i(\mathbf{r})]. \tag{3.21}$$

The $T_s[\rho_i(\mathbf{r})]$ term is the kinetic energy of the fictitious noninteracting system, the second term

$$U_{MF}[\rho_i] = \frac{V}{4}\int d\mathbf{r}\left(2\rho_3^2(\mathbf{r}) - 2\rho_0^2(\mathbf{r}) + \rho_1^2(\mathbf{r}) + \rho_2^2(\mathbf{r})\right) \tag{3.22}$$

is the mean-field approximation to the full particle-particle interaction $\langle\Psi_0|\hat{U}|\Psi_0\rangle$, and the third term, the exchange-correlation energy is defined as

$$F_{xc} \equiv \langle\Psi_0|\hat{T}+\hat{U}|\Psi_0\rangle - T_s - U_{MF} \tag{3.23}$$

which takes care of the rest part of the internal energy.

According to the second Hohenberg-Kohn theorem, the ground state energy is minimized by the ground state densities,

$$\begin{aligned}\frac{\partial E_g}{\partial\rho_i(\mathbf{r})} &= \frac{\partial T_s}{\partial\rho_i(\mathbf{r})} + \frac{\partial U_{\rm MF}}{\partial\rho_i(\mathbf{r})} + \frac{\partial F_{\rm xc}}{\partial\rho_i(\mathbf{r})} + W_i(\mathbf{r}) \\ &= \frac{\partial T_s}{\partial\rho_i(\mathbf{r})} + v_{i\rm MF}(\mathbf{r}) + v_{i\rm xc}(\mathbf{r}) + W_i(\mathbf{r})\end{aligned} \tag{3.24}$$

A noninteracting system subject to the effective potentials $v_{i\rm s}(\mathbf{r}) = v_{i\rm MF}(\mathbf{r}) + v_{i\rm xc}(\mathbf{r}) + W_i(\mathbf{r})$ would generate the same densities $\rho_i(\mathbf{r})$ as that of the interacting one. The Hamiltonian for the fictitious noninteracting system is

$$\hat{H}_s = \frac{1}{2}\int d\mathbf{r}\Phi_4^\dagger(\mathbf{r})\mathbf{H}_{\rm KS}(\mathbf{r})\Phi_4(\mathbf{r}), \tag{3.25}$$

where the four-component field operator $\Phi_4^\dagger(\mathbf{r}) = \begin{pmatrix} \psi_\uparrow^\dagger(\mathbf{r}) & \psi_\downarrow^\dagger(\mathbf{r}) & \psi_\uparrow(\mathbf{r}) & \psi_\downarrow(\mathbf{r}) \end{pmatrix}$ is a combination of particles and holes of different spins. The 4×4 Kohn-Sham matrix is given by

$$\mathbf{H}_{\rm KS} = \begin{pmatrix} h_\uparrow(\mathbf{r}) & 0 & 0 & v_{1s}(\mathbf{r}) - iv_{2s}(\mathbf{r}) \\ 0 & h_\downarrow(\mathbf{r}) & -(v_{1s}(\mathbf{r}) - iv_{2s}(\mathbf{r})) & 0 \\ 0 & -(v_{1s}(\mathbf{r}) + iv_{2s}(\mathbf{r})) & -h_\uparrow(\mathbf{r}) & 0 \\ (v_{1s}(\mathbf{r}) + iv_{2s}(\mathbf{r})) & 0 & 0 & -h_\downarrow(\mathbf{r}) \end{pmatrix} \tag{3.26}$$

with the spin-dependent single-particle Hamiltonian

$$h_\uparrow(\mathbf{r}) = -\frac{\nabla^2}{2m_\uparrow} + v_{3s}(\mathbf{r}) + v_{1s}(\mathbf{r}) \tag{3.27}$$

and

$$h_{\downarrow}(\mathbf{r}) = -\frac{\nabla^2}{2m_{\downarrow}} + v_{3s}(\mathbf{r}) - v_{1s}(\mathbf{r}). \tag{3.28}$$

3.3.2 Particle-hole symmetry

The Kohn-Sham matrix has an intrinsic particle-hole symmetry [58] which is expressed by

$$\Pi\, \mathbf{H}_{\mathrm{KS}} \Pi^{-1} = -\mathbf{H}_{\mathrm{KS}}. \tag{3.29}$$

The particle-hole operator has the form of a 4×4 matrix

$$\Pi = \begin{pmatrix} 0 & \mathbf{1} \\ \mathbf{1} & 0 \end{pmatrix} K \tag{3.30}$$

with K the complex conjugate operator and $\mathbf{1}$ the 2×2 unit matrix.

Due to this symmetry, for any eigenstate $|n_\alpha(\mathbf{r})\rangle$ of the Kohn-Sham matrix with eigen-energy $\epsilon_{n\alpha}$

$$\mathbf{H}_{\mathrm{KS}} |n_\alpha(\mathbf{r})\rangle = \epsilon_{n\alpha} |n_\alpha(\mathbf{r})\rangle, \tag{3.31}$$

there is a corresponding eigenstate $\tilde{n}_\alpha(\mathbf{r})\rangle \equiv \Pi |n_\alpha(\mathbf{r})\rangle$ with eigen-energy $-\epsilon_{n\alpha}$. Therefore, the solutions of the Kohn-Sham equations have the form

$$H_{\mathrm{KS}} \mathbf{U}_{n4}(\mathbf{r}) = \mathbf{U}_{n4}(\mathbf{r}) \begin{pmatrix} \epsilon_{n\uparrow} & 0 & 0 & 0 \\ 0 & \epsilon_{n\downarrow} & 0 & 0 \\ 0 & 0 & -\epsilon_{n\uparrow} & 0 \\ 0 & 0 & 0 & -\epsilon_{n\downarrow} \end{pmatrix} \tag{3.32}$$

where the 4×4 matrix $\mathbf{U}_{n4}(\mathbf{r}) \equiv (|n_\uparrow(\mathbf{r})\rangle |n_\downarrow(\mathbf{r})\rangle |\tilde{n}_\uparrow(\mathbf{r})\rangle |\tilde{n}_\downarrow(\mathbf{r})\rangle)$ is a combination of four eigenstates which are quasi-particle of spin up, quasi-particle of spin down, quasi-hole of spin up and quasi-hole of spin down, respectively. $\mathbf{U}_{n4}(\mathbf{r})$

is unitary if eigenstates $|n_\alpha(\mathbf{r})\rangle$ are all normalized. In other words, the Kohn-Sham matrix can be diagonalized by a generalized Bogoliubov transformation

$$\Phi_4(\mathbf{r}) = \sum_n \mathbf{U}_{n4}(\mathbf{r}) \begin{pmatrix} \gamma_{n\uparrow} \\ \gamma_{n\downarrow} \\ \gamma_{\tilde{n}\uparrow} \\ \gamma_{\tilde{n}\downarrow} \end{pmatrix} = \sum_n \mathbf{U}_{n4}(\mathbf{r}) \begin{pmatrix} \gamma_{n\uparrow} \\ \gamma_{n\downarrow} \\ \gamma^\dagger_{n\uparrow} \\ \gamma^\dagger_{n\downarrow} \end{pmatrix}. \tag{3.33}$$

Here we used the relation $\gamma_{\tilde{n}\alpha} = \gamma^\dagger_{n\alpha}$, which is a direct result of the particle-hole symmetry. In other words, adding a particle in the $|n_\alpha(\mathbf{r})\rangle$ state is equivalent as dragging a hole out of the $|\tilde{n}_\alpha(\mathbf{r})\rangle$ state.

The canonical anticommutation relations are invariant under the generalized Bogoliubov transformation,

$$\{\gamma^\dagger_{n\alpha}, \gamma_{m\beta}\} = \delta_{nm}\delta_{\alpha\beta}. \tag{3.34}$$

Thus the quasi-particles created by operators $\gamma^\dagger_{n\alpha}$ are fermionic.

After the diagonalization, the Kohn-Sham Hamiltonian becomes

$$\hat{H}_s = \frac{1}{2}\sum_{n\alpha} \epsilon_{n\alpha}(\gamma^\dagger_{n\alpha}\gamma_{n\alpha} - \gamma_{n\alpha}\gamma^\dagger_{n\alpha}) \tag{3.35}$$

with $\alpha = \uparrow, \downarrow$. The quasi-particle energy ϵ_{ni} can be either positive or negative. The ground state for the fictitious non-interacting system Ψ_{KS} is defined similar to the Dirac sea, with all the negative energy states occupied. Therefore one have $\gamma^\dagger_{n_\alpha}|\Psi_{\mathrm{KS}}\rangle = 0$ for $\epsilon_{n_\alpha} < 0$ and $\gamma_{n_\alpha}|\Psi_{\mathrm{KS}}\rangle = 0$ for $\epsilon_{n_\alpha} > 0$.

The Hamiltonian for the fictitious non-interacting system (3.31) could be further simplified by observing that the H_{KS} matrix could be decomposed

into two separate subblocks. One corresponds to spin-up particles and spin-down holes, and the other to spin-down particles and spin-up holes. Because the two subblocks are related by the particle-hole symmetry, it is sufficient to focus on one of them, say

$$H_{\mathrm{KS2}} = \begin{pmatrix} h_\uparrow(\mathbf{r}) & v_{1s}(\mathbf{r}) - iv_{2s}(\mathbf{r}) \\ v_{1s}(\mathbf{r}) + iv_{2s}(\mathbf{r}) & -h_\downarrow(\mathbf{r}) \end{pmatrix}. \tag{3.36}$$

Here the subscript 2 indicates that it is in the form a 2×2 matrix, therefore distinguishes it from the 4×4 Kohn-Sham matrix in (3.26).

The Kohn-Sham Hamiltonian is simplified as

$$\hat{H}_s = \int d\mathbf{r} \Phi_2^\dagger(\mathbf{r}) H_{\mathrm{KS2}}(\mathbf{r}) \Phi_2(\mathbf{r}) \tag{3.37}$$

with the two component spinor

$$\Phi_2(\mathbf{r}) = \begin{pmatrix} \psi_\uparrow(\mathbf{r}) \\ \psi_\downarrow^\dagger(\mathbf{r}) \end{pmatrix} \tag{3.38}$$

the same as the Nambu particle-hole spinor.

Compared to (3.25), the factor 1/2 disappears due to the redundancy from the particle-hole symmetry. Below, for brevity, we omit the subscript 2 in (3.36) and (3.38) when no confusion would likely arise.

The simplified 2×2 Kohn-Sham matrix is diagonalized by the corresponding 2×2 generalized Bogoliubov transformation matrix

$$\begin{pmatrix} \psi_\uparrow(\mathbf{r}) \\ \psi_\downarrow^\dagger(\mathbf{r}) \end{pmatrix} = \sum_n \mathbf{U}_n(\mathbf{r}) \begin{pmatrix} \gamma_{n\uparrow} \\ \gamma_{n\downarrow}^\dagger \end{pmatrix} \tag{3.39}$$

with $\mathbf{U}_n(\mathbf{r}) = (|n_\uparrow(\mathbf{r})\rangle, |\tilde{n}_\downarrow(\mathbf{r})\rangle)$. Here,

$$|n_\uparrow(\mathbf{r})\rangle = \begin{pmatrix} u_{n\uparrow}(\mathbf{r}) \\ v_{n\uparrow}(\mathbf{r}) \end{pmatrix} \quad and \quad |\tilde{n}_\downarrow(\mathbf{r})\rangle = \begin{pmatrix} v^*_{n\downarrow}(\mathbf{r}) \\ u^*_{n\downarrow}(\mathbf{r}) \end{pmatrix} \tag{3.40}$$

are the eigenstates of the 2×2 Kohn-Sham matrix, satisfying the Kohn-Sham equations

$$\hat{H}_{\rm KS}\mathbf{U}_n(\mathbf{r}) = \mathbf{U}_n(\mathbf{r}) \begin{pmatrix} \epsilon_{n\uparrow} & 0 \\ 0 & -\epsilon_{n\downarrow} \end{pmatrix} \tag{3.41}$$

The densities are given by

$$n_\uparrow(\mathbf{r}) = \sum_n \left(|u_{n_\uparrow}(\mathbf{r})|^2 \Theta(-\epsilon_{n_\uparrow}) + |v_{n_\downarrow}(\mathbf{r})|^2 \Theta(\epsilon_{n_\downarrow}) \right), \tag{3.42}$$

$$n_\downarrow(\mathbf{r}) = \sum_n \left(|u_{n_\downarrow}(\mathbf{r})|^2 \Theta(-\epsilon_{n_\downarrow}) + |v_{n_\uparrow}(\mathbf{r})|^2 \Theta(\epsilon_{n_\uparrow}) \right), \tag{3.43}$$

$$d(\mathbf{r}) = \sum_n \left(u_{n_\uparrow}(\mathbf{r}) v^*_{n_\uparrow}(\mathbf{r}) \Theta(\epsilon_{n_\uparrow}) + u_{n_\downarrow}(\mathbf{r}) v^*_{n_\downarrow}(\mathbf{r}) \Theta(-\epsilon_{n_\downarrow}) \right). \tag{3.44}$$

The Kohn-Sham equations reduce to (3.8) of the normal superfluids when the system is spin-unpolarized. The single particle Hamiltonian $h_\uparrow(\mathbf{r}) = h_\downarrow(\mathbf{r})$ is then spin-independent. Under this restriction, we can directly check that the time reversal symmetry is intrinsic in the 2×2 Kohn-Sham matrix (3.36), i.e.,

$$\mathbf{T} H_{\rm KS} \mathbf{T}^{-1} = -H_{\rm KS}, \tag{3.45}$$

where the time reversal operator $\mathbf{T} = i\tau_2 K$. Due to the time reversal symmetry, there is a two-fold degeneracy in the state from the Kramers' theorem. In other words, for any eigenstates $|n_\uparrow\rangle$, its time reversal counterpart $\mathbf{T}|n_\uparrow\rangle$ is also an eigenstate with energy $-\epsilon_{n_\uparrow}$. This leads to the degeneracy of the two energy bands of different spins, $\epsilon_{n_\uparrow}$ and $\epsilon_{n_\downarrow}$. Besides, we have $\gamma_{n_\uparrow} = \gamma_{n_\downarrow}$, the

generalized Bogoliubov transformation (3.39) is then reduced to the normal Bogoliubov transformation [59].

For given configuration of the external potentials, the densities could be solved out as functional of them through (3.42), (3.43) and (3.44), i.e., $\rho_i(\mathbf{r}) = \rho_i[W_j(\mathbf{r})]$. Generally, as basic variables describing the un-polarized superfluid system, the densities are independent. But this is based on the assumption that all the four $W_i(\mathbf{r})$ are adjustable parameters. If we fix the values of some number m of $W_i(\mathbf{r})$, $m \leq 4$, the four densities will no longer be independent, but confined to the m restrictions

$$W_j[\rho_i(\mathbf{r})] = C_j \tag{3.46}$$

with C_j some constants and $j = 1, \cdots m$. In other words, the number of degree of freedom is reduced to $4 - m$.

As an example of the reduced degree of freedom, let us study the BCS mean-field equations [15] which was firstly proposed by Leggett in his seminar paper [32]. The gap equation for the order parameter is

$$1 = -V \sum_k \frac{1}{2\epsilon_k} \tag{3.47}$$

and the density equation

$$n = \sum_k (1 - \frac{\eta_k}{\epsilon_k}) \tag{3.48}$$

with $\eta_k = \frac{k^2}{2} - \mu$ and $\epsilon_k = \sqrt{\eta_k^2 + \Delta^2}$. The BCS mean-field equations can be directly derived from (3.42), (3.43) and (3.44) as the results of applying

- spin symmetry: $v_{1s}(\mathbf{r}) = 0$ and $m_1 = m_2$;
- vanished external pair potential $W_1(\mathbf{r}) - iW_2(\mathbf{r}) = 0$;
- and homogeneous external particle potential $W_3(\mathbf{r}) = W_3$.

Only W_3 survives as an adjustable parameter with all the other $W_i(\mathbf{r})$ vanishes, so the number of degrees of freedom is reduced to 1. In the BCS mean-field equations, the uniform W_3 is absorbed into the chemical potential as $\mu - W_3 \to \mu$. We can see that both (3.47) and (3.48) provide relations between n, Δ and μ, therefore $\Delta(n)$ and $\mu(n)$ are no longer independent and can be solved out as function of n as shown in Figure 3.1.

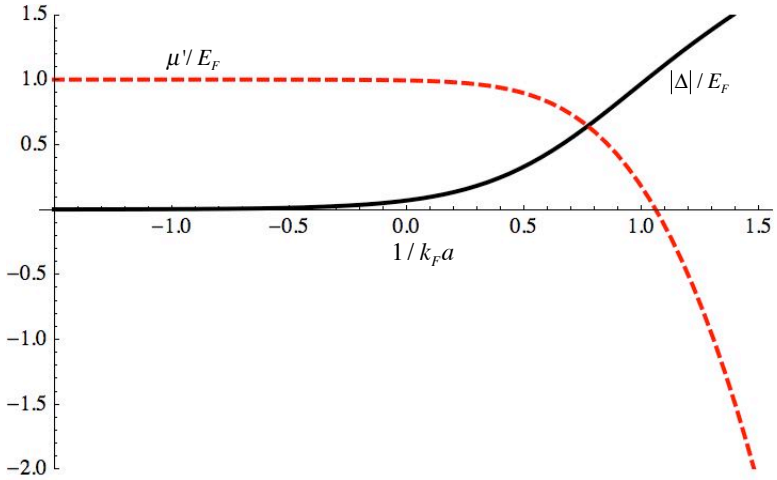

Figure 3.1: Chemical potential μ (red, dashed) and order parameter Δ (black, solid) as a function of the interaction strength $1/k_F a$ along the BCS-BEC crossover (in the units of non-interacting fermi energy $E_F = k_F^2/2$).

Chapter 4

Adiabatic Dynamics Theory

The time-dependent density functional theory (TDDFT)[60] is an extension of the time-independent (static) DFT to systems with time-dependent potentials. As the time-dependent version of the first Hohenberg-Kohn theorem, the Runge-Gross theorem shows that the time-dependent density is completely and exactly determined by the time-dependent external potential, and vice versa, as far as the initial condition of the system is given. In time-dependent systems, the total energy is no longer conserved as in the static system. Instead, the action integral which is defined as

$$A[n(\mathbf{r},t)] = \int_{t_0}^{t_1} dt \langle \Psi_0[n(\mathbf{r},t)](t)| i\frac{\partial}{\partial t} - \hat{H}(t)|\Psi_0[n(\mathbf{r},t)](t)\rangle \tag{4.1}$$

is stationary at the solutions of the time dependent Schrodinger equation.

The same as the static DFT, the time-dependent density is generated from a fictitious non-interacting system in which the density is equal to that of the original interacting system. The time-dependent Kohn-Sham equations, which are derived as the stationary point of the action integral with variation of the density $n(\mathbf{r},t)$, take the form

$$\left(-\frac{1}{2}\nabla^2 + v_s(\mathbf{r},t)\right)\psi_i(\mathbf{r},t) = i\frac{\partial}{\partial t}\psi_i(\mathbf{r},t) \tag{4.2}$$

with the initial condition $\psi_i(\mathbf{r}, 0) = \psi_i(\mathbf{r})$ and the effective potential v_s in the form of

$$v_s[n](\mathbf{r}, t) = v_{ext}(\mathbf{r}, t) + v_{MF}(\mathbf{r}, t) + v_{xc}(\mathbf{r}, t), \tag{4.3}$$

as functional of the density. The time-dependent density reads

$$n(\mathbf{r}, t) = \sum_{1}^{N} |\psi_i(\mathbf{r}, t)|^2. \tag{4.4}$$

While the TDDFT is exact without any spatial and temporal approximations, it is not suitable for practical calculations because technically a point at a certain position and time would have the memory of all the previous times and be effected by all the other points across the space. The adiabatic dynamical theory we will develop in this chapter only involves quantities which can be directly calculated from a static DFT, which is a great advantage compared to TDDFT.

4.1 Adiabatic equations of motion

In the adiabatic limit, Niu and Kleinman [61] proposed an exact method for the calculation of magnon dispersion curves based on the time-independent spin-DFT, as shown in Figure(4.1). The adiabatic dynamics of the spin waves is completely determined from the ground state energy and the Berry curvature terms, both of which are the properties of ground state and can be obtained from the standard time-independent spin-DFT method in a straightforward way. The Niu-Kleinman adiabatic dynamics is adopted here to study the spin-polarized superfluid system in the BEC-BCS crossover. We will show that both

the ground state energy and the Berry curvature, which are the only two terms involved in the adiabatic equations of motion, can be computed directly based on the static DFT for spin-polarized superfluid we developed in the previous chapter.

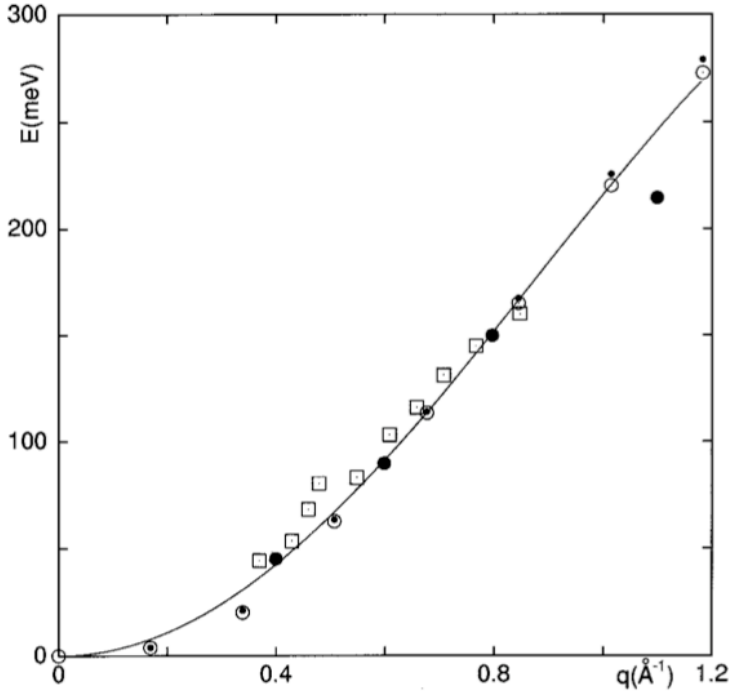

Figure 4.1: Magnon energies $\hbar\omega$ in meV vs wave vector. The squares are experimental data while the open circles are theoretical calculations from Niu-Kleinman adiabatic equations of motion. From [62].

One basic assumption of the adiabatic dynamics theory is that the time scale of the density dynamics $n(\mathbf{r}, t)$ is much larger than the time scale of the quasi-particles dynamics $\psi_i(\mathbf{r}, t)$ in (4.5). The quasi-particle wave functions can then instantaneously follow the slowly-varying density and the effective

potential field, namely

$$\left(-\frac{1}{2}\nabla^2 + v_s[n(\mathbf{r},t)]\right)\psi_i[n(\mathbf{r},t)](\mathbf{r}) = \epsilon_i[n(\mathbf{r},t)]\psi_i[n(\mathbf{r},t)]\mathbf{r}). \tag{4.5}$$

In other words, the whole Kohn-Sham system, including Hamiltonian, the quasi-particle wave function and the effective potential, depends on time only through the time-dependent density under the adiabaticity assumption. The degrees of freedom in the fast quasi-particle dynamics are completely ignored. The action integral in (4.1) now becomes

$$A[n(\mathbf{r},t)] = \int_{t_0}^{t_1} dt\langle\Psi[n(\mathbf{r},t)]|i\frac{\partial}{\partial t} - \hat{H}[n(\mathbf{r},t)]|\Psi[n(\mathbf{r},t)]\rangle. \tag{4.6}$$

For given density distribution at a certain time t, all the corresponding ground state properties, including the ground state energy $E_g[n(\mathbf{r},t)]$, the ground state wave function $|\Psi_a[n(\mathbf{r},t)]\rangle$ and the external particle potential $v[n(\mathbf{r},t)]$, could be calculated through the standard static DFT method. As we mentioned, the true solution of the time-dependent Schrodinger equation serves as a stationary point of the action integral (4.1), so the exact density $n(\mathbf{r},t)$ can be computed from the Euler equation

$$\frac{\partial A[n(\mathbf{r},t)]}{\partial n(\mathbf{r},t)} = 0. \tag{4.7}$$

The adiabatic approximation we adopted is essentially a projection operation, which restricts the dynamics of the system to the instantaneous ground state, as shown in Figure 4.2. As we see from Chapter 2, the energy of low-lying collective modes (density perturbations) is either sonic, with a gapless

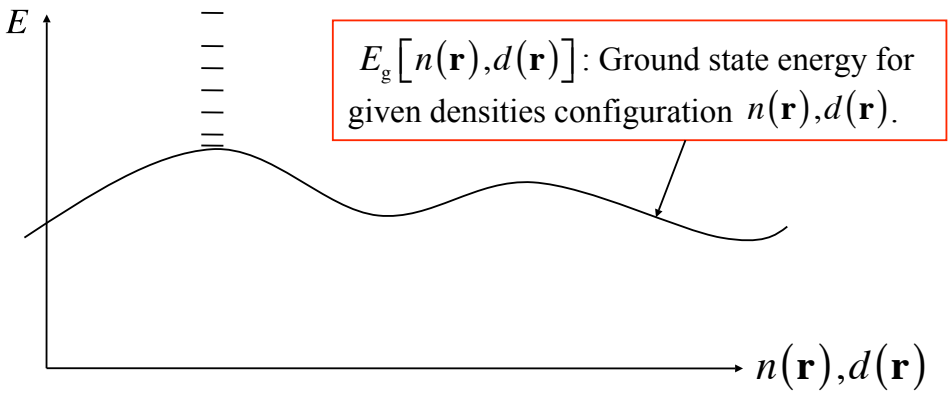

Figure 4.2: Image shows how the adiabatic evolution works

dispersion relation $\omega = ck$, or in the same order of trap frequency $\sqrt[3]{\omega_\perp^2 \omega_z}$ of the harmonic trap. In both cases, the adiabatic approximation holds.

It is straightforward to generalize the adiabatic dynamics theory from a normal DFT with only the particle density $n(\mathbf{r}, t)$ as the basic variable, to a DFT for spin-polarized superfluids with four density fields $\rho_i(\mathbf{r}, t)$. The variations are then independently taken with respect to $\rho_i(\mathbf{r}, t)$ in the ground state energy minimizing process , which leads to the Niu-Kleinman adiabatic equations of motion, namely

$$\frac{\partial E_g}{\partial \rho_i(\mathbf{r}, t)} - \sum_j \int d\mathbf{r}' \Omega_{ij}(\mathbf{r}, \mathbf{r}', t) \frac{d\rho_j(\mathbf{r}', t)}{dt} = 0 \tag{4.8}$$

where $E_g = \langle \Psi_a[\rho_i] | \hat{H} | \Psi_a[\rho_i] \rangle$ is the instantaneous ground state energy as functional of densities configuration $\rho_i(\mathbf{r}, t)$, while $\Omega_{ij}(\mathbf{r}, \mathbf{r}', t)$ defined as

$$\Omega_{ij}(\mathbf{r}, \mathbf{r}', t) = i\langle \frac{\partial \Psi_0}{\partial \rho_i(\mathbf{r}, t)} | \frac{\partial \Psi_0}{\partial \rho_j(\mathbf{r}', t)} \rangle - i\langle \frac{\partial \Psi_0}{\partial \rho_j(\mathbf{r}', t)} | \frac{\partial \Psi_0}{\partial \rho_i(\mathbf{r}, t)} \rangle \tag{4.9}$$

is the Berry curvature which normally appears in the description of adiabatic dynamics.

4.1.1 Ground state energy

A point that might cause confusion in the calculation of E_g is the external potential perturbations $W_{i1}(\mathbf{r})$. As we mentioned before, the low-lying collective mode we focus on is self-induced without the driving from time-dependent external potentials. This directly leads to all first order perturbations $W_{i1}(\mathbf{r}) = 0$. Therefore, in the calculation of ground state energy

$$E = F[\rho_{i0} + \rho_{i1}] + \sum_i \int d\mathbf{r} \left(W_{i0}(\mathbf{r}) - \mu\delta_{i3}\right)\left(\rho_{i0}(\mathbf{r}) + \rho_{i1}(\mathbf{r}, t)\right), \qquad (4.10)$$

the part of energy caused by the $W_{i1}(\mathbf{r}) = 0$ coupled to the densities is not counted. In this sense, the energy given in (4.10) is not the real ground state energy (we will call it the frozen energy) for density configuration $\rho_{i0} + \rho_{i1}$. It is the energy in a dynamical process with the the density perturbations present (with the internal energy $F[\rho_{i0} + \rho_{i1}]$) but self-excited (without W_{i1}). W_{i1} does not appear directly in (4.10), however, in order to evaluate the value of $F[\rho_{i0} + \rho_{i1}]$, it must be introduced in the Kohn-Sham equations (4.8) to calculate quasi-particle wave functions for given density perturbations ρ_{i1}.

The frozen energy defined in the form of (4.10) can be expressed as a

Taylor expansion up to second order of the density perturbations, namely

$$\begin{aligned} E &= F[\rho_{i0}] + \sum_i \int d\mathbf{r}\, (W_{i0}(\mathbf{r}) - \mu\delta_{i3})\, \rho_{i0}(\mathbf{r}) \\ &+ \sum_i \int d\mathbf{r} \left(\frac{\partial F[\rho_{i0}]}{\partial \rho_{i0}(\mathbf{r})} + W_{i0}(\mathbf{r}) - \mu\delta_{i3} \right) \rho_{i1}(\mathbf{r}, t) \\ &+ \sum_{ij} \int d\mathbf{r} d\mathbf{r}' \frac{\partial^2 F[\rho_{i0}]}{\partial \rho_{i0}(\mathbf{r}) \partial \rho_{j0}(\mathbf{r}')} \rho_{i1}(\mathbf{r}, t) \rho_{j1}(\mathbf{r}', t). \end{aligned} \tag{4.11}$$

The zeroth order is the ground state energy of the unperturbed system, which is minimized by the densities ρ_{i0},

$$\frac{\partial F[\rho_i]}{\partial \rho_i(\mathbf{r})} + W_{i0}(\mathbf{r}) - \mu\delta_{i3} = 0. \tag{4.12}$$

As a result of this, in the second line of (4.11), the first derivative of the ground state energy with respect ρ_{i0} vanishes. The second derivative

$$K_{ij}(\mathbf{r}, \mathbf{r}') \equiv \frac{\partial^2 E}{\partial \rho_{i0}(\mathbf{r}) \partial \rho_{j0}(\mathbf{r}')} = \frac{\partial^2 F}{\partial \rho_{i0}(\mathbf{r}) \partial \rho_{j0}(\mathbf{r}')} \tag{4.13}$$

which appears in the third line of (4.11) is positive definite.

4.1.2 Berry curvature

The Berry curvature was introduced by Berry in the study of adiabatic dynamics of quantum systems [63]. By definition in (4.9), the Berry curvature is anti-symmetric,

$$\Omega_{ji}(\mathbf{r}', \mathbf{r}) = -\Omega_{ij}(\mathbf{r}, \mathbf{r}') \tag{4.14}$$

and real

$$\Omega_{ij}^*(\mathbf{r}, \mathbf{r}') = \Omega_{ij}(\mathbf{r}, \mathbf{r}'). \tag{4.15}$$

Besides the differential formula given in (4.9), the Berry curvature can also be written as a summation over the interacting many-body states:

$$\Omega_{ij}(\mathbf{r},\mathbf{r}') = i\sum_{n\neq 0}\frac{\langle\Psi_0|\partial\hat{H}/\partial\rho_i(\mathbf{r})|\Psi_n\rangle\langle\Psi_n|\partial\hat{H}/\partial\rho_j(\mathbf{r}')|\Psi_0\rangle - [(i,\mathbf{r})\leftrightarrow(j,\mathbf{r}')]}{(E_{\Psi_n}-E_g)^2}. \tag{4.16}$$

The exact interacting ground state Ψ_0 is too difficult to reach, which is why the DFT is so useful and popular in the study of many-body systems. The DFT allows one to use the ground state densities $n(\mathbf{r})$ and $d(\mathbf{r})$ instead of Ψ_0. We follow the practice in the calculation of Berry curvature for electronic polarization [64], using Ψ_{KS} instead of Ψ_0 and $\hat{H}_s$ instead of $\hat{H}$ in (4.9) or (4.16). Here

$$\hat{H}_s = \int d\mathbf{r}\Phi^\dagger(\mathbf{r})\hat{H}_{\mathrm{KS}}\Phi(\mathbf{r}) \tag{4.17}$$

is the grand-canonical Hamiltonian for the noninteracting system [50].

4.1.3 External pair potential

In the same way as n is coupled to an external particle potential, or the spin-polarziation density is coupled to a magnetic field on a fixed direction, the anomalous density d is coupled to a pair potential.

The physical significance of the external pair potential $W_1 - iW_2$ is well-discussed in [46]. In a superfluid system, the internal interaction is long-ranged and gives rise to the well-known proximity effect in a clean contact between a superconductor and a normal metal. Thus, there should be a small induced order parameter on the normal side in a tunnel junction between

a superconductor and a normal metal, the same as the finite magnetization generated by a magnetic field **H** in a paramagnet.

4.2 Validity of adiabatic dynamics

It is worthy to emphasize that the adiabatic equations of motion (4.8) are built upon the adiabatic assumption that the densities $\rho_i(\mathbf{r}, t)$ are quantities slowly-varying in time compared to the fast-moving quasi-particles. A valid solution of (4.8) should be consistent with the adiabatic assumption. This is the reason why our study focuses on the low-lying collective modes in the BEC-BCS crossover, as written in the title of the dissertation. In the superfluid system (spin polarized or not), the existence of a low-lying mode is guaranteed by the Goldstone's theorem, which states the following [65]

> If the ground state breaks a continuous symmetry possessed by the Hamiltonian, there exists always low-energy excitations with dispersion $\omega_q = cq$.

The continuous symmetry being broken for superfluid (superconductors) is the global gauge symmetry, with respect to a global change in phase of the anomalous density $d(\mathbf{r}) \to e^{i\theta} d(\mathbf{r})$. The energy of the system remains unchanged when θ is shifted by an arbitrary amount, but there is huge ground-state degeneracy. When a particular value of θ is chosen in the ground state to break the gauge symmetry, necessarily a gapless collective mode will appear in the spectrum of possible excitations. This Goldstone mode is a

long-wavelength fluctuation of the corresponding order parameter. Some other examples of the Goldstone's theorem are the spin waves with rotation symmetry broken, phonon excitations in crystals with translational symmetry broken and pions with chiral symmetry broken.

This global gauge symmetry of superfluid system is broken with any external pair potential $W_1(\mathbf{r}) - iW_2(\mathbf{r})$ present, in the same way that the presence of a magnetic field would destroy the spatial rotation symmetry of the Hamiltonian, with a specified direction given by the magnetic field. The external pair potential appearing in the Hamitonian breaks the global gauge symmetry, with a specified gauge field

$$\theta(\mathbf{r}) = \tan^{-1}\left(\frac{-W_2(\mathbf{r})}{W_1(\mathbf{r})}\right). \tag{4.18}$$

In conclusion, a gapless excitation would appear as a result of the Goldstone's theorem if the Hamiltonian is globally gauge invariant, which means, the time scale of the dynamics of densities could be arbitrarily large. Therefore, if the global gauge symmetry is broken due to the presence of an external pair potential, or some other reasons (like an asymmetric confining potential), the validity of the equations of motion (4.8) should be consistent with the adiabatic assumption.

4.3 Linear assumption

Another assumption Niu and Kleinman employed to further simplify the adiabatic equations of motion (4.8) is the linear assumption. For densities

consisting of a fixed static part and a small time-dependent perturbation

$$\rho_i(\mathbf{r},t) = \rho_{i0}(\mathbf{r}) + \rho_{i1}(\mathbf{r},t), \tag{4.19}$$

the equations of motion (4.8) up to the first order of the perturbation reads

$$\sum_j \int d\mathbf{r}' \left(K_{ij0}(\mathbf{r},\mathbf{r}')\rho_{j1}(\mathbf{r}',t) - \Omega_{ij0}(\mathbf{r},\mathbf{r}')\frac{d\rho_{j1}(\mathbf{r}',t)}{dt} \right) = 0. \tag{4.20}$$

Here, the real and symmetric coefficient $K_{ij0}(\mathbf{r},\mathbf{r}')$ is defined as

$$K_{ij0}(\mathbf{r},\mathbf{r}') \equiv \left. \frac{\partial^2 E_g[\rho_i(\mathbf{r})]}{\partial\rho_{i1}(\mathbf{r},t)\partial\rho_{j1}(\mathbf{r}',t)} \right|_{\rho_{i1}(\mathbf{r},t)=0} = \frac{\partial^2 E_g[\rho_{i0}(\mathbf{r})]}{\partial\rho_{i0}(\mathbf{r})\partial\rho_{j0}(\mathbf{r}')}, \tag{4.21}$$

where the subscript in the second term means that $K_{ij0}(\mathbf{r},\mathbf{r}')$ is calculated in the limit where all the density perturbations $\rho_{i1}(\mathbf{r},t)$ vanish. Similarly, the real and anti-symmetric Berry curvature is defined as

$$\begin{aligned} \Omega_{ij0}(\mathbf{r},\mathbf{r}') &\equiv \left[i\langle \frac{\partial\Psi_0[\rho_i]}{\partial\rho_{i1}(\mathbf{r},t)} | \frac{\partial\Psi_0[\rho_i]}{\partial\rho_{j1}(\mathbf{r}',t)} \rangle - i\langle \frac{\partial\Psi_0[\rho_i]}{\partial\rho_{j1}(\mathbf{r}',t)} | \frac{\partial\Psi_0[\rho_i]}{\partial\rho_{i1}(\mathbf{r},t)} \rangle \right]_{\rho_{i1}(\mathbf{r},t)=0} \\ &= i\langle \frac{\partial\Psi_0[\rho_{i0}]}{\partial\rho_{i0}(\mathbf{r})} | \frac{\partial\Psi_0[\rho_{i0}]}{\partial\rho_{j0}(\mathbf{r}')} \rangle - i\langle \frac{\partial\Psi_0[\rho_{i0}]}{\partial\rho_{j0}(\mathbf{r}')} | \frac{\partial\Psi_0[\rho_{i0}]}{\partial\rho_{i0}(\mathbf{r})} \rangle. \end{aligned} \tag{4.22}$$

This result is exact in the adiabatic and small perturbation limit. Both Ω and K are ground state properties of the time-independent system which is completely determined by the densities $\rho_{i0}(\mathbf{r})$. We will call this system with $\rho_{i0}(\mathbf{r})$ the unperturbed system for simplicity. Furthermore, all the symmetries of the unperturbed symmetry will be expressed in the Ω and K matrix and therefore in the solutions of (4.20). We will discuss about this with more details later.

4.4 Static linear response theory

The density perturbations $\rho_{i1}(\mathbf{r},t)$ are induced by the perturbations of external potentials W_{i1}, or more directly, perturbations of the effective single-particle potentials v_{is1}. When the quasi-particle spectrum is gapped, the connections between ρ_{i1} and v_{is1} can be derived from the static linear response theory (perturbation theory) after some tedious but straightforward calculations

$$\rho_{i1}(\mathbf{r},t)=\sum_j\int d\mathbf{r}'v_{sj1}(\mathbf{r}',t)G_{ji}(\mathbf{r}',\mathbf{r}). \tag{4.23}$$

The linear response function $G_{ji}(\mathbf{r}',\mathbf{r})$ is real and symmetric,

$$\begin{aligned} G_{ij}(\mathbf{r},\mathbf{r}') &= \sum_{n_\alpha,m_\beta}\left(\frac{g_{jn_\alpha m_\beta}(\mathbf{r}')g_{im_\beta n_\alpha}(\mathbf{r})}{\epsilon_{m_\beta 0}-\epsilon_{n_\alpha 0}}\right)\left(\Theta(-\epsilon_{m_\beta 0})-\Theta(-\epsilon_{n_\alpha 0})\right) \\ &- \sum_{n_\alpha} g_{jn_\alpha n_\alpha}(\mathbf{r}')g_{in_\alpha n_\alpha}(\mathbf{r})\delta(\epsilon_{n_\alpha 0}) \end{aligned} \tag{4.24}$$

with $g_{jn_\alpha m_\beta}(\mathbf{r})=\langle n_{\alpha 0}(\mathbf{r})|\tau_j|m_{\beta 0}(\mathbf{r})\rangle$. Here, the eigenstates $|n_\uparrow\rangle=|n_1\rangle$ and $|n_\downarrow\rangle=|\tilde{n}_2\rangle$ with eigen-energies $\epsilon_{n\uparrow 0}=\epsilon_{n10}$ and $\epsilon_{n_\downarrow 0}=-\epsilon_{n20}$, respectively. The subscript 0 indicates the unperturbed system. Again, the linear response function $G_{ji}(\mathbf{r}',\mathbf{r})$ depends on the unperturbed system only. and inherits all its symmetries. Due to the one-to-one correspondence between ρ_{i1} and v_{is1}, the linear response function $G_{ji}(\mathbf{r}',\mathbf{r})$ is invertible. Mathematically, this invertibility leads to

$$v_{sj1}(\mathbf{r}',t)=\sum_i\int d\mathbf{r}\rho_{i1}(\mathbf{r},t)G^{-1}_{ji}(\mathbf{r}',\mathbf{r}) \tag{4.25}$$

as the inverse function of (4.23).

The K matrix, as defined by (4.13), is the sum of three parts: the contribution from the kinetic energy

$$T_s^{(2)} = \int d\mathbf{r}_1 d\mathbf{r}_2 \sum_{jj'} G_{ij}^{-1}(\mathbf{r}, \mathbf{r}_1) N_{jj'}(\mathbf{r}_1, \mathbf{r}_2) G_{j'i'}^{-1}(\mathbf{r}_2, \mathbf{r}') \tag{4.26}$$

with

$$N_{jj'}(\mathbf{r}_1, \mathbf{r}_2) = \sum_{n_\alpha m_\beta} g_{jn_\alpha m_\beta}(\mathbf{r}_1) g_{j'm_\beta n_\alpha}(\mathbf{r}_2) \left(\epsilon_{n_\alpha 0} \frac{\Theta(-\epsilon_{m_\beta 0}) - \Theta(-\epsilon_{n_\alpha 0})}{\left(\epsilon_{m_\beta 0} - \epsilon_{n_\alpha 0}\right)^2} \right), \tag{4.27}$$

the contribution from the mean-field approximation of the particle-particle interaction $U_{\mathrm{MF}}^{(2)}$ from (3.22), and the contribution from the exchange-correlation energy $F_{\mathrm{xc}}^{(2)}$ which depends on actual models beyond the DFT.

Finally, the Berry curvature matrix becomes

$$\Omega_{ii'}(\mathbf{r}, \mathbf{r}') = \sum_{jj'} \int d\mathbf{r}_1 d\mathbf{r}_2 G_{ij}^{-1}(\mathbf{r}, \mathbf{r}_1) O_{jj'}(\mathbf{r}_1, \mathbf{r}_2) G_{j'i'}^{-1}(\mathbf{r}_2, \mathbf{r}') \tag{4.28}$$

with the real function

$$O_{jj'}(\mathbf{r}_1, \mathbf{r}_2) = i \sum_{n_\alpha m_\beta} g_{jn_\alpha m_\beta}(\mathbf{r}_1) g_{j'm_\beta n_\alpha}(\mathbf{r}_2) \frac{\Theta(\epsilon_{m_\beta 0}) \Theta(-\epsilon_{n_\alpha 0})}{\left(\epsilon_{m_\beta 0} - \epsilon_{n_\alpha 0}\right)^2} + c.c. \,. \tag{4.29}$$

In this chapter, we have developed a general formalism for the adiabatic dynamics of a spin-polarized fermionic superfluid in the BEC-BCS crossover, which is exact in the adiabatic limit. Since the hydrodynamic theory breaks down with the local density approximation, this adiabatic dynamics theory, which bypasses LDA, serves as a useful tool in the investigation of the dynamical behaviors in the BEC-BCS crossover. In general cases, numerical

simulations of standard DFT techniques are needed to carry out the calculation. As an analytical application, we will study the uniform superfluid system which is analytically soluable in the next chapter.

.

Chapter 5

Adiabatic Dynamics in the Uniform System

In this section, we will study a uniform superfluid system where

- $W_0(\mathbf{r})$, $W_3(\mathbf{r})$ and the modulus of external pair potential $W_p(\mathbf{r}) = |W_1(\mathbf{r}) - iW_2(\mathbf{r})|$ are homogeneous, and
- the external pair potential phase $\theta(\mathbf{r}) = \mathbf{P} \cdot \mathbf{r}$ only depends on a constant molecular center of momentum $\mathbf{P}$.

A uniform superfluid system is one of the very few cases where the self-consistent Kohn-Sham equations (3.41) are analytically solvable. These analytical results will help us to have a deeper understanding of the low-lying collective modes in the BEC-BCS crossover. Most importantly, we will show that our adiabatic equations of motion (4.8) will be reduced to the hydrodynamic equation of motion (2.2) within the local density approximation.

5.1 Solutions of adiabatic equations of motion

A uniform system is invariant under spatial translation of the form $\mathbf{r} \to \mathbf{r} + \mathbf{a}$ for arbitrary displacement $\mathbf{a}$. Due to this continuous translational symmetry, the coefficients $K(\mathbf{r}, \mathbf{r}')$ and $\Omega(\mathbf{r}, \mathbf{r}')$ appearing in the adiabatic

equations of motion (4.20) only depend on the relative coordinates $\mathbf{r}-\mathbf{r}'$, namely

$$K_{ij}(\mathbf{r},\mathbf{r}') = K_{ij}(\mathbf{r}-\mathbf{r}') \qquad \text{and} \qquad \Omega_{ij}(\mathbf{r},\mathbf{r}') = \Omega_{ij}(\mathbf{r}-\mathbf{r}'). \tag{5.1}$$

Hence (4.20) can be greatly simplified as

$$\sum_j \left(K_{ij\mathbf{k}} + i\omega_{\mathbf{k}}\Omega_{ij\mathbf{k}}\right)\rho_{j\mathbf{k}1} = 0 \tag{5.2}$$

with $K_{ij\mathbf{k}}$, $\Omega_{ij\mathbf{k}}$ and $\rho_{j\mathbf{k}1}$ the fourier components of $K_{ij}(\mathbf{r}-\mathbf{r}')$, $\Omega_{ij}(\mathbf{r}-\mathbf{r}')$ and $\rho_{j1}(\mathbf{r},t)$, respectively. Here, we have also replaced the time derivative by $-i\omega_{\mathbf{k}}$. We can see from (5.2) that the matrices $K_{ij\mathbf{k}}$ and $\Omega_{ij\mathbf{k}}$ decompose into separate 4×4 subblocks according to the different values of the wave vector $\mathbf{k}$.

By definition, the function $K_{ij}(\mathbf{r}-\mathbf{r}')$ is real and symmetric while the Berry curvature $\Omega_{ij}(\mathbf{r}-\mathbf{r}')$ is real and anti-symmetric. This directly leads to the following relationships among their fourier components:

$$K_{ij\mathbf{k}} = K^*_{ij(-\mathbf{k})}, \qquad K_{ij\mathbf{k}} = K_{ji(-\mathbf{k})} \tag{5.3}$$

and

$$\Omega_{ij\mathbf{k}} = \Omega^*_{ij(-\mathbf{k})}, \qquad \Omega_{ij\mathbf{k}} = -\Omega_{ji(-\mathbf{k})}. \tag{5.4}$$

In another word, $K_{ij\mathbf{k}}$ is hermitian while $\Omega_{ij\mathbf{k}}$ is anti-hermitian. Specially, K_{ij0} is symmetric while Ω_{ij0} is anti-symmetric in the limit where $\mathbf{k}=0$.

A further simplification occurs when we assume that the external pair potential modulus W_p vanishes. This is a practical assumption since no external pair potential is applied in the set up of current experiments. However, the

external pair potential phase $\theta(\mathbf{r}) = \mathbf{P} \cdot \mathbf{r}$ is kept to drive a uniform superfluid flow with molecular center of momentum $\mathbf{P}$. The superfluid system is still global gauge invariant since $W_p \to 0$. This is a little tricky and can be better understood with an analogy with a ferromagnetic system. The spatial rotation symmetry of a ferromagnet is broken with the presence of a magnetic field. Spins prefer to align themselves with the magnetic field, and will gradually change direction to fit with a slowly varying magnetic field in space. At the limit where the magnetic field vanishes, the energy of the ferromagnetic system with a spatial-changing spin distribution is still rotationally invariant. In a superfluid system, the order parameter phase is induced by the phase of the external pair potential. Once a superfluid flow is generated by external pair potential, it will not fade off. In the real experiments, a superfluid flow may be excited by some other practical ways, but mathematically, the superfluid velocity is related to the gradient of order parameter phase, which is induced by the phase of external pair potential.

Due to the gauge invariance, the existence of gapless collective mode is guaranteed by Goldstone's theorem. The degree of freedom for the system variables (Δ, n, m and $\theta(\mathbf{r})$) is reduced to 3 as W_p vanishes. The order parameter modulus Δ (or equivalently, modulus of anomalous density) will be function of the other three, n, m and $\theta(\mathbf{r})$ (or $\mathbf{P} = \nabla\theta$).

In a uniform system where the continuous wave vector $\mathbf{k}$ serves as the energy level index, a finite spin polarization density $m(\mathbf{r})$ is achieved when either of the two particle bands has intersections with the chemical potential,

or equivalently, when either $\epsilon_{1\mathbf{k}0}$ or $\epsilon_{2\mathbf{k}0}$ (3.41) is negative in some regions of momentum space. The quasi-particle spectrum is then gapless, which would violate the adiabatic assumption that the quasi-particles have much smaller time scales and would immediately follow the instantaneous configurations of density perturbation excited. In the real cases, the energy level index n is discrete in the presence of some confining potentials. Or the two particle bands would be split up into Bloch bands separated by energy gaps with a periodic potential applied. In either cases, a finite $m(\mathbf{r})$ could be achieved together with a gapped quasi-particle spectrum, where our adiabatic dynamics theory is still applicable.

Since we will focus on the adiabatic dynamics of a uniform superfluid system in this section, we assume that both v_{s0} and m vanish and the particle bands have no intersections with the chemical potential. The degree of freedom for the system variables is then reduced to 2. We define that the effective pair potential $v_{1s}-iv_{2s} = v_{sp}e^{i\theta(\mathbf{r})}$ with v_{sp} as the modulus. The Kohn-Sham matrix for the unperturbed system takes the form

$$H_{\mathrm{KS}} = \begin{pmatrix} \dfrac{(-i\nabla)^2}{2m_1} + v_{s3} - \mu & v_{sp}e^{i\theta(\mathbf{r})} \\ v_{sp}e^{-i\theta(\mathbf{r})} & -\left(\dfrac{(-i\nabla)^2}{2m_2} + v_{s3} - \mu\right) \end{pmatrix}. \tag{5.5}$$

In the following discussions, we will always choose the gauge where the effective

pair potential is real. The Kohn-Sham matrix becomes

$$H_{\mathrm{KS}} = \begin{pmatrix} \frac{\left(-i\nabla + \frac{\mathbf{P}}{2}\right)^2}{2m_1} + v_{s3} - \mu & v_{sp} \\ v_{sp} & -\left(\frac{\left(-i\nabla - \frac{\mathbf{P}}{2}\right)^2}{2m_2} + v_{s3} - \mu\right) \end{pmatrix}. \quad (5.6)$$

The Kohn-Sham equations (3.41) with Hamiltonian (5.6) have plane wave solutions, namely

$$|\mathbf{k}_{10}\rangle = \begin{pmatrix} U_{\mathbf{k}} \\ V_{\mathbf{k}} \end{pmatrix} e^{i\mathbf{k}\cdot r} \qquad \text{and} \qquad |\tilde{\mathbf{k}}_{20}\rangle = \begin{pmatrix} -V_{\mathbf{k}} \\ U_{\mathbf{k}} \end{pmatrix} e^{i\mathbf{k}\cdot r} \quad (5.7)$$

with corresponding eigen-energy

$$\epsilon_{\mathbf{k}_{1,2}0} = \epsilon_{\mathbf{k}} \pm \frac{\xi_{1\mathbf{k}} - \xi_{2\mathbf{k}}}{2} \quad (5.8)$$

respectively. Here, $\xi_{1,2\mathbf{k}} = (\mathbf{k} \pm \mathbf{P}/2)^2/(2m_{1,2}) + v_{3s} - \mu$ are the single particle energies for different spins. $\epsilon_{\mathbf{k}} = \sqrt{S_{\mathbf{k}}^2 + v_{sp}^2}$ with $S_{\mathbf{k}} = (\xi_{1\mathbf{k}} + \xi_{2\mathbf{k}})/2$. The coefficients appearing in the quasi-particle wave functions are real

$$U_{\mathbf{k}} = \sqrt{\frac{\epsilon_{\mathbf{k}} + S_{\mathbf{k}}}{2\epsilon_{\mathbf{k}}}} \qquad \text{and} \qquad V_{\mathbf{k}} = \sqrt{\frac{\epsilon_{\mathbf{k}} - S_{\mathbf{k}}}{2\epsilon_{\mathbf{k}}}} \quad (5.9)$$

and resemble similar forms of the usual BCS occupation coefficients.

The densities can be self-consistently expressed by the quasi-particle wave functions as in (3.42), (3.43) and (3.44), namely

$$n = \sum_{\mathbf{k}} 2V_{\mathbf{k}}^2 \quad (5.10)$$

$$d = \sum_{\mathbf{k}} U_{\mathbf{k}} V_{\mathbf{k}}. \quad (5.11)$$

We can see that the unperturbed d is real and its first order perturbation

$$d_1(\mathbf{r}) \equiv (d + d_{A1}(\mathbf{r}))\, e^{i\theta_1(\mathbf{r})} - d = d_{A1}(\mathbf{r}) + i\, d\, \theta_1(\mathbf{r}) \tag{5.12}$$

has an imaginary part which is proportional to the phase perturbation $\theta_1(\mathbf{r})$. Here, $d_{A1}(\mathbf{r})$ represents the amplitude perturbation of d while $\theta_1(\mathbf{r})$ represents phase perturbation.

For given values of n and $\mathbf{P}$, the effective chemical potential $\mu - v_{s3}$ together with d can be solved out as function of them with an appropriate approximation for the exchange-correlation energy $F_{xc}(n, \mathbf{P})$ (3.23). We then substitute these values into the adiabatic equation of motion (5.2), and calculate the corresponding collective mode energy $\omega_{\mathbf{k}}$ and perturbation distribution $\rho_{i\mathbf{k}1}$ as function of the parameters n and $\mathbf{P}$.

5.2 Symmetries and invariance

Before we deal with any real numbers, we will firstly see how far we can go to solve the adiabatic equations of motion from the intrinsic properties of the superfluid system and some relevant symmetries.

The adiabatic equations of motion (5.2) are mathematically equations of 2×2 matrices. We are interested in its solutions in the long wavelength limit where $\mathbf{k} \to 0$. We expand $\Omega_{ij\mathbf{k}}$ around the point $\mathbf{k} = 0$, and get $\Omega_{ij\mathbf{k}} = \Omega_{ij0} + \Omega^{(1)}_{ij\mathbf{k}}$ up to the first order of $\mathbf{k}$. Ω_{ij0} is real and anti-symmetric as we mentioned before, namely

$$\begin{pmatrix} 0 & \Omega_{230} \\ -\Omega_{230} & 0 \end{pmatrix}. \tag{5.13}$$

We can also derive directly from the anti-hermiticity of $\Omega_{ij\mathbf{k}}$ (5.4) that its first order expansion $\Omega^{(1)}_{ij\mathbf{k}}$ is imaginary and symmetric. A further study shows that $\Omega^{(1)}_{22\mathbf{k}}$ vanishes due to the gauge invariance.

Similarly, $K_{ij\mathbf{k}} = K_{ij0} + K^{(1)}_{ij\mathbf{k}} + K^{(2)}_{ij\mathbf{k}}$ up to the second order of $\mathbf{k}$. The reason we keep $K_{ij\mathbf{k}}$ up to the second order is that the collective mode frequency $\omega_{\mathbf{k}}$, which times with $\Omega_{ij\mathbf{k}}$ in (5.2), is gapless and in the first order of $\mathbf{k}$.

K_{ij0} is real and symmetric. Since $\rho_{21}(\mathbf{r}) = 2d_{I1}(\mathbf{r}) = 2d\theta_1(\mathbf{r})$, its fourier component at the point $\mathbf{k} = 0$ is given by $\rho_{201} = 2d\theta_{01}$, which is proportional to a uniform gauge change θ_{01}. Due to the gauge invariance, element $K_{ij0} = 0$ if either the subscript i or j is 2. The matrix K_{ij0} takes the form

$$\begin{pmatrix} 0 & 0 \\ 0 & K_{330} \end{pmatrix}. \tag{5.14}$$

Due to the hermiticity of $K_{ij\mathbf{k}}$, $K^{(1)}_{ij\mathbf{k}}$ is imaginary and anti-symmetric while $K^{(2)}_{ij\mathbf{k}}$ is real and symmetric.

Apply all these simplifications obtained from the intrinsic properties of a uniform superfluid system onto the adiabatic equations of motion (5.2), we have that $\omega_{\mathbf{k}}$ will be the solution of an quadratic equation

$$a_{\mathbf{k}}\omega^2_{\mathbf{k}} + b_{\mathbf{k}}\omega_{\mathbf{k}} + c_{\mathbf{k}} = 0 \tag{5.15}$$

with the quadratic coefficient $a_{\mathbf{k}} = -(\Omega_{230})^2$, the linear coeffcient $b_{\mathbf{k}} = 2K^{(1)}_{23\mathbf{k}}\Omega_{230}$ and the constant term $c_{\mathbf{k}} = K_{330}K^{(2)}_{22\mathbf{k}} + (K^{(1)}_{23\mathbf{k}})^2$. The corresponding density

perturbations are given by

$$\begin{pmatrix} P_{\mathbf{k}1} \\ \rho_{3\mathbf{k}1} \end{pmatrix} = \begin{pmatrix} P^{(1)}_{\mathbf{k}1} \\ \\ \rho^{(1)}_{3\mathbf{k}1} \end{pmatrix} = \begin{pmatrix} \dfrac{ik}{2d}\dfrac{K_{330}}{K^{(1)}_{23\mathbf{k}} + i\Omega_{230}\omega_{\mathbf{k}}} \\ \\ 1 \end{pmatrix}, \tag{5.16}$$

where the momentum perturbation $P_{\mathbf{k}1} = ik/(2d)\rho_{2\mathbf{k}1}$. Both $P_{\mathbf{k}1}$ and $\rho_{3\mathbf{k}1}$ have vanished uniform perturbations.

Generally, we have two branches of the gapless collective modes as the solutions of (5.15), which are

$$\omega_{\mathbf{k}} = \frac{iK^{(1)}_{23\mathbf{k}}}{\Omega_{230}} \pm \frac{\sqrt{K_{330}K^{(2)}_{22\mathbf{k}}}}{|\Omega_{230}|}. \tag{5.17}$$

The two modes will be reduced to one if either a time-reversal symmetry or a spatial reversal symmetry is present, in either case, $\mathbf{P} = 0$. With a spatial reversal symmetry, all the first order expansion terms around $\mathbf{k} = 0$ disappear. While with a time reversal symmetry, $\Omega_{ij\mathbf{k}} = 0$ for even $i + j$ and $K_{ij\mathbf{k}} = 0$ for odd $i + j$. In either case, the first term in (5.17) vanishes, and $\omega_{\mathbf{k}}$ is reduced to

$$\omega_{\mathbf{k}} = \pm\frac{\sqrt{K^{(2)}_{22\mathbf{k}}K_{330}}}{|\Omega_{230}|} \tag{5.18}$$

with the corresponding density perturbations

$$\begin{pmatrix} P^{(1)}_{\mathbf{k}1} \\ \\ \rho^{(1)}_{3\mathbf{k}1} \end{pmatrix} = \begin{pmatrix} \dfrac{k}{2\,d\,\omega_{\mathbf{k}}}\dfrac{K_{330}}{\Omega_{230}} \\ \\ 1 \end{pmatrix}. \tag{5.19}$$

Four terms appear in the final solutions of the adiabatic equations of motion, $K^{(2)}_{22\mathbf{k}}$, K_{330}, $K^{(1)}_{23\mathbf{k}}$ and the Berry curvature Ω_{230}. Firstly,

$$K_{330} = \frac{\partial^2 F[n_0, \mathbf{P_0}]}{\partial n_0^2} = \frac{\partial \mu_0(n_0, \mathbf{P}_0)}{\partial n_0} \tag{5.20}$$

with subscript 0 represents values in the unperturbed system is a direct result of (4.12) and (4.13). Now we do some tricky calculation of $K^{(1)}_{23\mathbf{k}}$ from the definition

$$K_{23}(\mathbf{r},\mathbf{r}') \equiv \frac{\partial^2 F}{\partial\rho_2(\mathbf{r})\partial n(\mathbf{r}')} = \frac{1}{2d}\frac{\partial^2 F}{\partial\theta(\mathbf{r})\partial n(\mathbf{r}')}. \tag{5.21}$$

The internal energy F is functional of $n(\mathbf{r})$ and $\mathbf{P}(\mathbf{r}) = \nabla\theta(\mathbf{r})$ is the gradient of $\theta(\mathbf{r})$, therefore

$$K_{23}(\mathbf{r},\mathbf{r}') = \frac{1}{2d}\frac{\partial^2 F[n(\mathbf{r}),\nabla\theta(\mathbf{r})]}{\partial\theta(\mathbf{r})\partial n(\mathbf{r}')} = -\frac{1}{2d}\nabla_{\mathbf{r}}\cdot\left(\frac{\partial^2 F[n(\mathbf{r}),\nabla\theta(\mathbf{r})]}{\partial(\nabla\theta(\mathbf{r}))\partial n(\mathbf{r}')}\right). \tag{5.22}$$

In the limit where the density perturbations vanish,

$$K_{23}(\mathbf{r}-\mathbf{r}') = -\frac{1}{2d}\nabla_{\mathbf{r}}\cdot\left(\frac{\partial^2 F[n_0,\mathbf{P_0}]}{\partial\mathbf{P}_0\partial n_0}\delta(\mathbf{r}-\mathbf{r}')\right). \tag{5.23}$$

Straightforwardly, its fourier component $K_{23\mathbf{k}}$ vanishes at $\mathbf{k}=0$, and the first order expansion

$$K^{(1)}_{23\mathbf{k}} = -\frac{i\mathbf{k}}{2d}\cdot\frac{\partial F(n_0,\mathbf{P}_0)}{\partial n_0\partial\mathbf{P}_0} = -\frac{i\mathbf{k}}{2d}\cdot\frac{\partial\mu_0(n_0,\mathbf{P}_0)}{\partial\mathbf{P}_0} \tag{5.24}$$

or equivalently,

$$K^{(1)}_{23\mathbf{k}} = -\frac{i\mathbf{k}}{4d}\cdot\frac{\partial\mathbf{J}_s(n_0,\mathbf{P}_0)}{\partial n_0}, \tag{5.25}$$

where $\mathbf{J}_s \equiv \partial F/\partial(\mathbf{P}/2)$ is the superfluid particle current. [1] For a system

[1] By analytical mechanics it is found that variations δF due to variations of vector potential $\delta\mathbf{A}$ is given by

$$\delta F = -q\int d\mathbf{r}\mathbf{J}\cdot\delta\mathbf{A}$$

The momentum $\mathbf{P}$ acts as a vector potential in (5.6) with the substitution $\mathbf{P} = -2q\mathbf{A}$. Then it is straightforward to get that

$$\mathbf{J} = \frac{\partial F}{\partial(-q\mathbf{A})} = \frac{\partial F}{\partial(\mathbf{P}/2)}$$

described by (5.6), the superfluid particle current can be directly calculated as

$$\mathbf{J} = \sum_{\mathbf{k}} V_{\mathbf{k}}^2 \left(\frac{1}{m_1} \left(\frac{\mathbf{P}}{2} + \mathbf{k} \right) + \frac{1}{m_2} \left(\frac{\mathbf{P}}{2} - \mathbf{k} \right) \right). \tag{5.26}$$

In other words, a heavy atom with mass m_1 and momentum $\mathbf{k}+\mathbf{P}/2$ is paired to a light one having mass m_2 and momentum $-\mathbf{k}+\mathbf{P}/2$. The superfluid particle current as usual consists of two parts [66]: a diamagnetic part

$$\frac{n}{2} \left(\frac{\mathbf{P}}{2m_1} + \frac{\mathbf{P}}{2m_2} \right) \equiv \frac{n}{m_+} \frac{\mathbf{P}}{2} \tag{5.27}$$

which is always in the same direction as $\mathbf{P}$, and a paramagnetic part

$$\sum_{\mathbf{k}} V_{\mathbf{k}}^2 \left(\frac{\mathbf{k}}{m_1} + \frac{\mathbf{k}}{m_2} \right) \equiv \sum_{\mathbf{k}} 2V_{\mathbf{k}}^2 \frac{\mathbf{k}}{m_-} \tag{5.28}$$

which is in the opposite direction to $\mathbf{P}$. For equal masses $m_1 = m_2$, $V_{\mathbf{k}}$ as defined in (5.9) is independent of the direction of $\mathbf{k}$. As a direct consequence, the paramagnetic current will vanish.

Similarly, one can also show that

$$K_{22\mathbf{k}}^{(2)} = \frac{1}{4d^2} (\mathbf{kk}) \cdot \left(\frac{\partial^2 F[n_0, \mathbf{P_0}]}{\partial \mathbf{P}_0 \partial \mathbf{P}_0} \right), \tag{5.29}$$

which is reducible to a scalar

$$K_{22\mathbf{k}}^{(2)} = \frac{k^2}{4d^2} \frac{\partial^2 F[n_0, \mathbf{P_0}]}{\partial P_0^2} = \frac{k^2}{16d^2} \frac{\partial J_s[n_0, \mathbf{P_0}]}{\partial (P_0/2)}, \tag{5.30}$$

since $F[n_0, \mathbf{P_0}]$ is independent of the direction of $\mathbf{P}$.

The Berry curvature

$$\Omega_{230} = \frac{1}{2d} \left[i \langle \frac{\partial \Psi_0[n_0, \theta(\mathbf{r})]}{\partial \theta_1} | \frac{\partial \Psi_0[n_0, \theta(\mathbf{r})]}{\partial n_0} \rangle - i \langle \frac{\partial \Psi_0[n_0, \theta(\mathbf{r})]}{\partial n_0} | \frac{\partial \Psi_0[n_0, \theta(\mathbf{r})]}{\partial \theta_1} \rangle \right]_{\theta_1 = 0}, \tag{5.31}$$

can be calculated directly from the alternative definition of Berry curvature (4.16), which is simply (readers are refered to Appendix B for more details),

$$\Omega_{230} = \frac{1}{4d}. \tag{5.32}$$

With all the four terms related to physical quantities, the gapless collective spectrum turns out to be more meaningful, which is

$$\omega_{\mathbf{k}} = \left(\frac{\partial J_s}{\partial n_0} \hat{\mathbf{k}} \cdot \hat{\mathbf{P}}_0 \pm \sqrt{\frac{\partial \mu}{\partial n_0} \frac{\partial J_s}{\partial (P_0/2)}} \right) k \tag{5.33}$$

with superfluid particle current $J_s(n_0, P_0)$ and chemical potential $\mu(n_0, P_0)$ as functions of n_0 and P_0, defined as first derivatives of $F[n_0, P_0]$ with respect to $P_0/2$ and n_0, accordingly. The corresponding perturbations now become

$$\begin{pmatrix} P^{(1)}_{\mathbf{k}1}/2 \\ n^{(1)}_{\mathbf{k}1} \end{pmatrix} = \begin{pmatrix} \pm\sqrt{\frac{\partial^2 F}{\partial n_0^2} \Big/ \frac{\partial F}{\partial (P_0/2)^2}} \\ 1 \end{pmatrix}. \tag{5.34}$$

5.3 Derivation of hydrodynamic equations of motion

In this section, we will show that the adiabatic equation of motion (4.8), which is exact in the adiabatic and harmonic limit, will be reduced to the hydrodynamic equation of motion within the local density approximation. This provides a solid microscopic foundation for the phenomenological hydrodynamic theory in the whole region of BEC-BCS crossover.

Within the local density approximation, the internal energy $F[n(\mathbf{r}), P(\mathbf{r})]$ (where the square brackets indicate that the influence of external potentials

have been taken into account), as functional of spatial varying $n(\mathbf{r})$ and $P(\mathbf{r})$, is defined as

$$F[n(\mathbf{r}), P(\mathbf{r})] = F(n(\mathbf{r}), P(\mathbf{r})) + \int d\,\mathbf{r} n(\mathbf{r}) V_{ex}(\mathbf{r}). \tag{5.35}$$

where $F(n, P)$ is the internal energy of a uniform system in the absence of external potentials, and $V_{ex}(\mathbf{r})$ describe a spatial varying potential coupled to $n(\mathbf{r})$.

The dynamics of $\theta(\mathbf{r})$ is governed by the adiabatic equations of motion as

$$\int d\mathbf{r}' \left(K_{n\theta 0}(\mathbf{r}, \mathbf{r}')\theta_1(\mathbf{r}', t) + K_{nn0}(\mathbf{r}, \mathbf{r}')n_1(\mathbf{r}', t) - \Omega_{n\theta 0}(\mathbf{r}, \mathbf{r}')\frac{d\theta(\mathbf{r}', t)}{dt} \right) = 0, \tag{5.36}$$

where the first two terms (within the integration) can be combined as

$$\frac{\partial F[n(\mathbf{r}), P(\mathbf{r})]}{\partial n(\mathbf{r})} = \mu(n(\mathbf{r}), P(\mathbf{r})) + V_{ex}(\mathbf{r}). \tag{5.37}$$

The Berry curvature appearing in the third term $\Omega_{n\theta 0}(\mathbf{r}, \mathbf{r}')$ is calculated in the same way as (5.32), which turns out be $\Omega_{n\theta 0}(\mathbf{r}, \mathbf{r}') = -(1/2)\delta(\mathbf{r} - \mathbf{r}')$. We apply these results into (5.36), and take the gradient on both sides of the equation. We then have

$$-\nabla \left(\mu(n(\mathbf{r}), P(\mathbf{r})) + V_{ex}(\mathbf{r}) \right) = \frac{d}{dt} \left(\frac{\mathbf{P}(\mathbf{r}, t)}{2} \right), \tag{5.38}$$

which is the Euler's equation in the hydrodynamic theory.

Similarly, the adiabatic dynamics for $n(\mathbf{r})$ takes the form

$$\int d\mathbf{r}' \left(K_{\theta n0}(\mathbf{r}, \mathbf{r}')n_1(\mathbf{r}', t) + K_{\theta\theta 0}(\mathbf{r}, \mathbf{r}')\theta_1(\mathbf{r}', t) - \Omega_{\theta n0}(\mathbf{r}, \mathbf{r}')\frac{dn(\mathbf{r}', t)}{dt} \right) = 0 \tag{5.39}$$

with the first two terms (with the integration) combined as

$$\frac{\partial F(n(\mathbf{r}),P(\mathbf{r}))}{\partial\theta(\mathbf{r})}=-\nabla\cdot\left(\frac{\partial F(n(\mathbf{r}),P(\mathbf{r}))}{\partial\mathbf{P}(\mathbf{r})}\right)=-\frac{1}{2}\nabla\cdot\mathbf{J}_s(n(\mathbf{r}),P(\mathbf{r})). \quad (5.40)$$

This gives out the other part of Hydrodynamic equations of motion, the continuity equation

$$\frac{dn(\mathbf{r},t)}{dt}+\nabla\cdot\mathbf{J}_s(n(\mathbf{r}),P(\mathbf{r}))=0. \quad (5.41)$$

The hydrodynamic equations of motion we derived seems slightly different from the conventional one in (2.2), which we rewrite here for comparison,

$$\begin{aligned}\frac{\partial n}{\partial t} &= -\nabla\cdot(n\mathbf{v}), &(5.42)\\ \frac{d\mathbf{v}}{dt} &= -\nabla\left(V(\mathbf{r},t)+\mu(n(\mathbf{r},t))+\frac{v^2}{2}\right). &(5.43)\end{aligned}$$

In the conventional hydrodynamic theory, the particle current J_s is explicitly expressed as $n\mathbf{v}$, and the chemical potential $\mu(n,P)$ is split into two parts: a part only depends on $\mu(n)$ and the other part only on the velocity $v^2/2$. There the two equations (2.2) form a complete set for n and $\mathbf{v}$. Our hydrodynamic equations of motion, (5.38) and (5.41), is also complete since both $\mu(n,P)$ and $J_s(n,P)$ are totally determined by n and P. Besides, it is expressed in a more compact way, namely

$$\begin{aligned}\frac{\partial n}{\partial t} &= -\nabla\cdot\left(\frac{\partial F}{\partial\left(\mathbf{P}/2\right)}\right) &(5.44)\\ \frac{\partial\left(\mathbf{P}/2\right)}{\partial t} &= -\nabla\left(\frac{\partial F}{\partial n}\right) &(5.45)\end{aligned}$$

where $F=F[n(\mathbf{r}),P(\mathbf{r})]$ is given in (5.37).

Furthermore, (5.45) is more general since it includes cases where there is an interplay between n and P, and $\mu(n, P)$ can not simply be split into two separate parts, each depending on one of the two variables respectively.

Chapter 6

Conclusion

To investigate the adiabatic dynamics of low-lying collective modes in the BEC-BCS crossover, we first developed a density-functional theory specially formalized for a superfluid system with spin-polarization. Similar to the traditional DFT, which provides a description of normal systems in terms of the particle density $n(\mathbf{r})$; a superfluid system with spin-polarization can be completely and in principle exactly described in terms of four real fields. In additional to the normal $n(\mathbf{r})$, two order parameters, including a spin-polarization density $m(\mathbf{r})$ and a complex anomalous density $d(\mathbf{r})$, also serve as basic variables. A set of exact Kohn-Sham type equations are derived which are the generalization of the Bogoliubov-de Gennes equations to include the spin-polarization effects.

Based on this static DFT for spin-polarized superfluid, we then develop a general formalism for the adiabatic dynamics in the BEC-BCS crossover, which is exact in the adiabatic limit. With a further harmonic approximation, we show that the adiabatic dynamics is completely governed by properties of the original unperturbed system, and therefore may be greatly simplified if some symmetries are present in the unperturbed system. All the coefficients

in the adiabatic equations of motion are explicitly given from static linear response theory. The computational complexity of our formalism is the same as that of a static DFT, therefore the adiabatic dynamic theory is easier and more practical compared to methods based on the time-dependent DFT or Green function.

In general cases, applications of the adiabatic dynamic theory are carried out through numerical simulations with standard DFT techniques. As an analytical application, we study the adiabatic dynamics of a uniform superfluid system. An analytical investigation would, as we expect, deepen our understanding of the low-lying collective modes. We also show that the adiabatic equations of motion are reduced to the hydrodynamic equations of motion within local density approximation in a spin-unpolarized superfluid system. This gives a solid microscopic foundation to the well-publicized phenomenological hydrodynamic theory.

Appendices

Appendix A

One-to-one mapping between general densities and external potentials

In this appendix, I will show that there is a one-to-one mapping between the set of general densities $\{\rho_i(\mathbf{r})\}$ (or equivalently, the basic variables, $n(\mathbf{r})$, $m(\mathbf{r})$, $d_R(\mathbf{r})$ and $d_I(\mathbf{r})$) and the set of external potentials $\{W_i(\mathbf{r})\}$. The proof is a straightforward generalization of Hohenberg and Kohn's arguments in their seminar paper[47].

Firstly, the Hamiltonian of a spin-polarized superfluid system, as given in (3.16), is a functional of the four external potentials. Secondly, the ground state wave-function $|\Phi_0\rangle$ of this system, is the eigenfunction of the Schrodinger equation with the lowest energy

$$\hat{H}|\Phi_0\rangle = E_g|\Phi_0\rangle. \tag{A.1}$$

Thirdly, the four general densities can be calculated as the expectation values in the ground state, as in (3.11). Therefore, for given $\{W_i(\mathbf{r})\}$, $\{\rho_i(\mathbf{r})\}$ are uniquely determined.

To establish a one-to-one mapping between $\{\rho_i(\mathbf{r})\}$ and $\{W_i(\mathbf{r})\}$, we also need to show that the mapping $F : \{W_i(\mathbf{r})\} \rightarrow\{\ \rho_i(\mathbf{r})\}$ is invertible. We assume that there are two sets of different external potentials $\{W_i(\mathbf{r})\}$

and $\{W_i'(\mathbf{r})\}$ mapped to the same set of general densities $\{\rho_i(\mathbf{r})\}$. The corresponding Hamiltonian, ground state energy and ground state wave function associated with $\{W_i(\mathbf{r})\}$ and $\{W_i'(\mathbf{r})\}$ are represented by $\hat{H}$, E_g, $|\Phi_0\rangle$ and $\hat{H}'$, E_g', $|\Phi_0'\rangle$ accordingly. By the definition of ground state energy, we have

$$\begin{aligned} E_g' &= \langle\Phi_0'|\hat{H}'|\Phi_0'\rangle < \langle\Phi_0|\hat{H}'|\Phi_0\rangle = \langle\Phi_0|\left(\hat{H}+\hat{W}'-\hat{W}\right)|\Phi_0\rangle \\ &= E_g + \sum_i \rho_i(\mathbf{r})\left(W_i'(\mathbf{r}) - W_i(\mathbf{r})\right) \end{aligned} \tag{A.2}$$

Similarly, we also have

$$\begin{aligned} E_g &= \langle\Phi_0|\hat{H}|\Phi_0\rangle < \langle\Phi_0'|\hat{H}|\Phi_0'\rangle = \langle\Phi_0'|\left(\hat{H}'+\hat{W}-\hat{W}'\right)|\Phi_0'\rangle \\ &= E_g' + \sum_i \rho_i(\mathbf{r})\left(W_i(\mathbf{r}) - W_i'(\mathbf{r})\right) \end{aligned} \tag{A.3}$$

Adding (A.2) and (A.3) together leads to the paradox

$$E_g' + E_g < E_g + E_g'. \tag{A.4}$$

This shows that the mapping F is invertible, $\exists\ F^{-1} : \{\rho_i(\mathbf{r})\} \rightarrow\{\ W_i(\mathbf{r})\}$, therefore the ground state wave-function is completely determined by the set of general densities $\{\rho_i(\mathbf{r})\}$.

The arguments above are based on the assumption that the ground state is non-degenerate. For more general proof, please refer to [67].

Appendix B

Calculation of Berry Curvature Ω_{230}

We will adopt the alternative definition of Berry curvature as given in (4.16), where the excited states with n quasi-particles $|\Psi_n\rangle$ are defined as the Ground state $|\Psi_{KS}\rangle$ acted by n quasi-particle operators $\gamma^\dagger_{mi}$. It is assumed that all the quasi-particles have positive energies, thus

$$\langle\Psi_{KS}|\partial H_s/\partial\rho_i|\Psi_n\rangle = \langle\tilde{\mathbf{k}}_{20}|\partial H_{KS}/\partial\rho_i|\mathbf{k}_{10}\rangle \tag{B.1}$$

which is finite if only $|\Psi_n\rangle = \gamma^\dagger_{\mathbf{k}_{10}}\gamma^\dagger_{\tilde{k}_{20}}|\Psi_{KS}\rangle$.

The Berry curvature Ω_{230}, as defined in (5.31), is given by

$$\Omega_{230} = \frac{1}{2d}\left(i\sum_{\mathbf{k}}\frac{\langle\tilde{\mathbf{k}}_{20}|\partial H_{KS}/\partial\theta|\mathbf{k}_{10}\rangle\langle\mathbf{k}_{10}|\partial H_{KS}/\partial n|\tilde{\mathbf{k}}_{20}\rangle}{\left(\epsilon_{\mathbf{k}10}+\epsilon_{\mathbf{k}20}\right)^2}+c.c.\right)_{\theta=0} \tag{B.2}$$

with the Kohn-Sham matrix H_{KS} as in (5.6). A direct calculation shows that

$$\langle\tilde{\mathbf{k}}_{20}|\partial H_{KS}/\partial\theta|\mathbf{k}_{10}\rangle_{\theta=0} = -iv_{sp} \tag{B.3}$$

while

$$\langle\tilde{\mathbf{k}}_{20}|\partial H_{KS}/\partial n|\mathbf{k}_{10}\rangle_{\theta=0} = 2U_{\mathbf{k}}V_{\mathbf{k}}\frac{\partial\left(\mu-v_{s3}\right)}{\partial n}+\left(U^2_{\mathbf{k}}-V^2_{\mathbf{k}}\right)\frac{\partial v_{sp}}{\partial n} \tag{B.4}$$

Substitute these values into (B.2), we obtain

$$\Omega_{230} = \frac{1}{2d}\left(C\frac{\partial\left(\mu-v_{s3}\right)}{\partial n}+B\frac{\partial v_{sp}}{\partial n}\right) \tag{B.5}$$

with the constants $C = \sum_{\mathbf{k}} v_{sp}^2/(2\epsilon_{\mathbf{k}}^3)$ and $B = \sum_{\mathbf{k}} v_{sp} S_{\mathbf{k}}/(2\epsilon_{\mathbf{k}}^3)$.

Both the quantity $\mu - v_{s3}$ and v_{sp} are functions of n and P, as given in (5.10) and (5.11). Here, a further assumption for F_{xc} (3.23) is needed to relate d and v_{sp}. For simplicity, we assume that F_{xc} is independent of d, and v_{sp} is equal to d. The derivatives of $\mu - v_{s3}$ and v_{sp} with respect to n can be directly calculated from (5.10) and (5.11), which turns out to be

$$\frac{\partial\,(\mu - v_{s3})}{\partial n} = \frac{C}{2(B^2 + C^2)} \quad \text{and} \quad \frac{\partial v_{s1}}{\partial n} = \frac{B}{2(B^2 + C^2)} \tag{B.6}$$

Apply these values into (B.5), we get $\Omega_{230} = 1/(4d)$. Furthermore, $\Omega_{\theta n0} = 1/2$.

Bibliography

[1] S. N. Bose, *Plancks gesetz und lichtquantenhypothese*, Z. Phys. **26**, 178 (1924).

[2] A. Einstein, *Quantentheorie des einatomigen idealen Gases* (Berlin: Akademie-Verlag, 1925).

[3] M. H. Anderson, J. R. Ensher, M. R. Matthews, C. E. Wieman, and E. A. Cornell, *Observation of bose-einstein condensation in a dilute atomic vapor*, Science **269**, 198 (1995).

[4] C. C. Bradley, C. A. Sackett, J. J. Tollett, and R. G. Hulet, *Evidence of bose-einstein condensation in an atomic gas with attractive interactions*, Phys. Rev. Lett. **75**, 1687 (1995).

[5] K. B. Davis, M. O. Mewes, M. R. Andrews, N. J. van Druten, D. S. Durfee, D. M. Kurn, and W. Ketterle, *Bose-einstein condensation in a gas of sodium atoms*, Phys. Rev. Lett. **75**, 3969 (1995).

[6] J. Bardeen, L. N. Cooper, and J. R. Schrieffer, *Theory of superconductivity*, Phys. Rev. **108**, 1175 (1957).

[7] L. N. Cooper, *Bound electron pairs in a degenerate fermi gas*, Phys. Rev. **104**, 1189 (1956).

[8] M. Greiner, C. A. Regal, and D. S. Jin, *Emergence of a molecular bosee-instein condensate from a fermi gas*, Nature **426**, 537 (2003).

[9] S. Jochim, M. Bartenstein, A. Altmeyer, G. Hendl, S. Riedl, C. Chin, J. H. Denschlag, and G. Grimm, *Bose-einstein condensation of molecules*, Science **302**, 2101 (2003).

[10] M. W. Zwierlein, C. A. Stan, C. H. Schunck, S. M. F. Raupach, S. Gupta, Z. Hadzibabic, and W. Ketterle, *Observation of bose-einstein condensation of molecules*, Phys. Rev. Lett. **91**, 250401 (2003).

[11] T. Bourdel, L. Khaykovich, J. Cubizolles, J. Zhang, F. Chevy, M. Teichmann, L. Tarruell, S. J. J. M. F. Kokkelmans, and C. Salomon, *Experimental study of the bec-bcs crossover region in lithium 6*, Phys. Rev. Lett. **93**, 050401 (2004).

[12] G. B. Partridge, K. E. Strecker*, R. I. Kamar, M. W. Jack, and R. G. Hulet, *Molecular probe of pairing in the bec-bcs crossover*, Phys. Rev. Lett. **95**, 020404 (2005).

[13] C. Regal, M. Greiner, and D. S. Jin, *Observation of resonance condensation of fermionic atom pairs*, Phys. Rev. Lett. **92**, 040403 (2004).

[14] M. W. Zwierlein, C. A. Stan, C. H. Schunck, S. M. F. Raupach, A. J. Kerman, and W. Ketterle, *Condensation of pairs of fermionic atoms near a feshbach resonance*, Phys. Rev. Lett. **92**, 120403 (2004).

[15] S. Giorgini, L. P. Pitaevskii, and S. Stringari, *Theory of ultracold atomic fermi gases*, Rev. Mod. Phys. **80**, 1215 (2008).

[16] M. Greiner, C. A. Regal, and D. S. Jin, *Fermi condensates*, arXiv:cond-mat/0502539v1 (2005).

[17] U. Fano, *Effects of configuration interaction on intensities and phase shifts*, Phys. Rev. **124**, 1866 (1961).

[18] H. Feshbach, *A unified theory of nuclear reactions. ii*, Annals of Physics **19**, 287 (1962).

[19] T. Bourdel, J. Cubizolles, L. Khaykovich, K. M. F. Magalhaes, S. J. J. M. F. Kokkelmans, G. V. Shlyapnikov, and C. Salomon, *Measurement of the interaction energy near a feshbach resonance in a ^{6}li fermi gas*, Phys. Rev. Lett. **91**, 020402 (2003).

[20] M. W. Zwierlein, J. R. Abo-Shaeer, A. Schirotzek, C. H. Schunck, and W. Ketterle, *Vortices and superfluidity in a strongly interacting fermi gas*, Nature **435**, 1047 (2005).

[21] Q. Chen, J. Stajic, S. Tan, and K. Levin, *Bcs-bec crossover: From high temperature superconductors to ultracold superfluids*, Physics Reports **412**, 1 (2005).

[22] A. Gezerlis and J. Carlson, *Strongly paired fermions: Cold atoms and neutron matter*, Phys. Rev. C **77**, 032801 (2008).

[23] K. M. O'Hara, S. L. Hemmer, M. E. Gehm, S. R. Granade, and J. E. Thomas, *Observation of a strongly interacting degenerate fermi gas of atoms*, Science **298** (2002).

[24] M. Bartenstein, A. Altmeyer, S. Riedl, S. Jochim, C. Chin, J. H. Denschlag, and R. Grimm, *Collective excitations of a degenerate gas at the bec-bcs crossover*, Phys. Rev. Lett. **92**, 203201 (2004).

[25] J. Kinast, S. Hemmer, M. E. Gehm, A. Turlapov, and J. E. Thomas, *Evidence for superfluidity in a resonantly interacting fermi gas*, Phys. Rev. Lett. **92**, 150402 (2004).

[26] C. Menotti, P. Pedri, and S. Stringari, *Expansion of an interacting fermi gas*, Phys. Rev. Lett. **89**, 250402 (2002).

[27] J. Joseph, B. Clancy, L. Luo, J. Kinast, A. Turlapov, and J. E. Thomas, *Measurement of sound velocity in a fermi gas near a feshbach resonance*, Phys. Rev. Lett. **98**, 170401 (2007).

[28] S. Stringari, *Collective oscillations of a trapped superfluid fermi gas near a feshbach resonance*, Europhys. Lett. **65**, 749 (2004).

[29] M. Inguscio, W. Ketterle, and C. Salomon, *Gas di fermi ultrafreddi* (IOS Press, 2007).

[30] Y. Ohashi and A. Griffin, *Superfluidity and collective modes in a uniform gas of fermi atoms with a feshbach resonance*, Phys. Rev. A **67**, 063612 (2003).

[31] Y. Ohashi and A. Griffin, *Single-particle excitations in a trapped gas of fermi atoms in the bcs-bec crossover region*, Phys. Rev. A **72**, 013601 (2005).

[32] A. J. Leggett, *Diatomic molecules and cooper pairs*, Modern trends in the theory of condensed matter, Lecture Notes in Physics **115**, 13 (1980).

[33] G. E. Astrakharchik, J. Boronat, J. Casulleras, and S. Giorgini, *Equation of state of a fermi gas in the bec-bcs crossover: A quantum monte carlo study*, Phys. Rev. Lett. **93**, 200404 (2004).

[34] M. Bartenstein, *From Molecules to Cooper Pairs: Experiments in the BEC-BCS crossover* (Universitt Innsbruck, 2005).

[35] P. Pieri, L. Pisani, and G. Strinati, *Bcs-bec crossover at finite temperature in the broken-symmetry phase*, Phys. Rev. B **70**, 094508 (2004).

[36] Q. Chen, J. Stajic, and K. Levin, *Thermodynamics of interacting fermions in atomic traps*, Phys. Rev. Lett. **95**, 260405 (2005).

[37] R. Haussmann, W. Rantner, S. Cerrito, and W. Zwerger, *Thermodynamics of the bcs-bec crossover*, Phys. Rev. A **75**, 023610 (2007).

[38] N. Manini and L. Salasnich, *Bulk and collective properties of a dilute fermi gas in the bcs-bec crossover*, Phys. Rev. A **71**, 033625 (2005).

[39] Y. Castin and R. Dum, *Bose-einstein condensates in time dependent traps*, Phys. Rev. Lett. **77**, 5315 (1996).

[40] C. J. Pethick and H. Smith, *Bose-Einstein condensation in dilute gases* (Cambridge University Press, 2002).

[41] E. Burovski, E. Kozik, N. Prokof'ev, B. Svistunov, and M. Troyer, *Critical temperature curve in bec-bcs crossover*, Phys. Rev. Lett. **101**, 090402 (2008).

[42] A. Altmeye, S. Riedl, C. Kohstall, M. J. Wright, R. Geursen, M. Bartenstein, C. C. amd J. H. Denschlag, and R. Grimm, *Precision measurements of collective oscillations in the bec-bcs crossover*, Phys. Rev. Lett. **98**, 040401 (2007).

[43] G. B. Partridge, W. Li, R. I. Kamar, Y. A. Liao, and R. G. Hulet, *Pairing and phase separation in a polarized fermi gas*, Science **311**, 503 (2006).

[44] Y. Shin, M. W. Zwierlein, C. H. Schunck, A. Schirotzek, and W. Ketterle, *Observation of phase separation in a strongly interacting imbalanced fermi gas*, Phys. Rev. Lett. **97**, 030401 (2006).

[45] G. B. Partridge, W. Li, Y. A. Liao, R. G. Hulet, M. Haque, and H. T. C. Stoof, *Deformation of a trapped fermi gas with unequal spin populations*, Phys. Rev. Lett. **97**, 190407 (2006).

[46] L. N. Oliveira, E. K. U. Gross, and W. Kohn, *Density-functional theory for superconductors*, Phys. Rev. Lett. **60**, 2430 (1988).

[47] P. Hohenberg and W. Kohn, *Inhomogeneous electron gas*, Phys. Rev. **136**, B864 (1964).

[48] W. Kohn and L. Sham, *Self-consistent equations including exchange and correlation effects*, Phys. Rev. **140**, A1133 (1965).

[49] N. D. Mermin, *Thermal properties of the inhomogeneous electron gas*, Phys. Rev. **137**, A1441 (1965).

[50] C. Fiolhais, F. Nogueira, and M. Marques, *A primer in density functional theory* (Springer, 2003).

[51] W. Kohn, *Nobel lecture: Electronic structure of matterwave functions and density functionals*, Rev. Mod. Phys. **71**, 1253 (1999).

[52] A. Rajagopal and J. Callaway, *Inhomogeneous electron gas*, Phys. Rev. B **7**, 1912 (1973).

[53] O. Gunnarsson and B. I. Lundqvist, *Exchange and correlation in atoms, molecules, and solids by the spin-density-functional formalism*, Phys. Rev. B **13**, 4274 (1976).

[54] U. von Barth and L. Hedin, *A local exchange-correlation potential for the spin polarized case. i*, Journal of Physics C: Solid State Physics **5**, 1629 (1972).

[55] S. Kurth, M. Marques, M. Lüders, and E. Gross, *Local density approximation for superconductors*, Phys. Rev. Lett. **83**, 2628 (1999).

[56] Y. Nambu and G. Jona-Lasinio, *Dynamical model of elementary particles based on an analogy with superconductivity. i*, Phys. Rev. **122**, 345 (1961).

[57] Y. Nambu and G. Jona-Lasinio, *Dynamical model of elementary particles based on an analogy with superconductivity. ii*, Phys. Rev. **124**, 246 (1961).

[58] A. Altland and M. Zirnbauer, *Nonstandard symmetry classes in mesoscopic normal-superconducting hybrid structures*, Phys. Rev. B **55**, 1142 (1997).

[59] P.-G. de Gennes, *Superconductivity of metals and alloys* (Perseus Books, 1999).

[60] E. Runge and E. Gross, *Density-functional theory for time-dependent systems*, Phys. Rev. Lett. **52**, 997 (1984).

[61] Q. Niu and L. Kleinman, *Spin-wave dynamics in real crystals*, Phys. Rev. Lett. **80**, 2205 (1998).

[62] D. M. Bylander, Q. Niu, and L. Kleinman, *Fe magnon dispersion curve calculated with the frozen spin-wave method*, Phys. Rev. B **61**, R11875 (2000).

[63] M. V. Berry, *Quantal phase factors accompanying adiabatic changes*, Proceedings of the Royal Society **392**, 45 (1984).

[64] R. Resta, *Macroscopic polarization in crystalline dielectrics: the geometric phase approach*, Rev. Mod. Phys. **66**, 899 (1994).

[65] T.-K. Ng, *Introduction to classical and quantum field theory* (Wiley-VCH, 2009).

[66] M. Tinkham, *Introduction to superconductivity* (McGraw-Hill, New York, 1996).

[67] F. Bassani, F. Fumi, and M. P. Tosi, *Highlights of condensed-matter theory: proceedings of the International School of Physics "Enrico Fermi"* (Elsevier Science Publishing Company Inc., 1985).

[68] Q. Niu, X. Wang, L. Kleinman, W. Liu, D. M. C. Nicholson, and G. M. Stocks, *Adiabatic dynamics of local spin moments in itinerant magnets*, Phys. Rev. Lett. **83**, 207 (1999).

[69] P. W. Anderson, *Random-phase approximation in the theory of superconductivity*, Phys. Rev. **112**, 1900 (1958).

[70] K. Y. M. Wong and S. Takada, *Effects of quasiparticle screening on collective modes. ii. superconductors*, Phys. Rev. B **37**, 5644 (1988).

[71] A. Messiah, *Quantum mechanics* (Courier Dover Publications, 1999).

[72] P. Pieri and G. C. Strinati, *Strong-coupling limit in the evolution from bcs superconductivity to bose-einstein condensation*, Phys. Rev. B **61**, 15370 (2000).

[73] M. Holland, S. J. J. M. F. Kokkelmans, M. L. Chiofalo, and R. Walser, *Resonance superfluidity in a quantum degenerate fermi gas*, Phys. Rev. Lett. **87**, 120406 (2001).

[74] L. P. Gor'kov, *Mikroskopicheskoe proiskhozhdenie uravnenii ginzburga landau v teorii sverkhprovodimosti*, Zh. Eksp. Teor. Fiz. **36**, 1918 (1959).

[75] V. L. Ginzburg and L. D. Landau, *On the theory of superconductivity*, Zh. Eksp. Teor. Fiz. **20**, 1064 (1950).

[76] T. N. D. Silva and E. J. Mueller, *Surface tension in unitary fermi gases with population imbalance*, Phys. Rev. Lett. **97**, 070402 (2006).